actuators

Active Control of Bluff-Body Flows Using Plasma Actuators

Efstathios Konstantinidis [ID]

Department of Mechanical Engineering, University of Western Macedonia, 50132 Kozani, Greece;
ekonstantinidis@uowm.gr; Tel.: +30-24610-56754

Abstract: Actuators play an important role in modern active flow control technology. Dielectric barrier discharge plasma can be used to induce localized velocity perturbations in air, so as to accomplish modifications to the global flow field. This paper presents a selective review of applications from the published literature with emphasis on interactions between plasma-induced perturbations and original unsteady fields of bluff-body flows. First, dielectric barrier discharge (DBD)-plasma actuator characteristics, and the local disturbance fields these actuators induce into the exterior flow, are described. Then, instabilities found in separated flows around bluff bodies that controlled actuation should target at are briefly presented. Key parameters for effective control are introduced using the nominally two-dimensional flow around a circular cylinder as a paradigm. The effects of the actuator configuration and location, amplitude and frequency of excitation, input waveform, as well as the phase difference between individual actuators are illustrated through examples classified based on symmetry properties. In general, symmetric excitation at frequencies higher than approximately five times the uncontrolled frequency of vortex shedding acts destructively on regular vortex shedding and can be safely employed for reducing the mean drag and lift fluctuations. Antisymmetric and symmetric excitation at low frequencies of the order of the natural frequency can amplify the wake instability and increase the mean and fluctuating aerodynamic forces, respectively, due to vortex locking-on to the excitation frequency or its subharmonics. Results from several studies show that the geometry and arrangement of the electrodes is of utmost significance. Power consumption is typically very low, but the electromechanical efficiency can be optimized by input waveform modulation.

Keywords: flow control; dielectric barrier discharge; zero-net mass flux; cylinder wakes; vortex shedding

1. Introduction

Flow control denotes the use of various methods to manipulate the natural state of a fluid flow to have desired properties for a specific purpose. The ability to control flows can be beneficial in many engineering and science applications. Effective flow control can be used to reduce aerodynamic drag; increase the maneuverability of vehicles, including road, airborne, and underwater vehicles; lower noise generation from objects moving at high speeds; augment heat transfer and mixing in industrial processes; accelerate reaction rates in chemical and biochemical reactors; enhance cooling of devices such as electronic chips, compressors, and turbine blades; improve the efficiency of internal combustion engines and devices that harness the kinetic energy of wind and water currents; suppress unwanted flow-induced vibrations of overhead lines and offshore pipelines, etc. In turn, achieving these targets helps reduce fuel consumption and pollutant emissions, lower the risk of industrial accidents, and prolong the life expectancy of structural components, which highlights the economic, environmental, and societal potential of active flow control (AFC) technologies.

Actuators play an important role in AFC technology. Fluidic actuators are devices that can inject fluid momentum, remove fluid momentum, or both through tiny slots in the walls of a solid body, with the objective being to control exterior flow characteristics. This era begun with the pioneering work of Prandtl, who demonstrated that separation of the boundary layer in various flows, including those over a circular cylinder, can be delayed by applying steady suction on the surface [1]. In the modern era, steady as well as unsteady suction and blowing are commonly employed in AFC [2]. During the last 2–3 decades, actuator technology has been progressing at a fast pace, as witnessed by the development of synthetic-jet and plasma actuators, which can be driven by fast electronic circuits [3–5]. The main advantage of these actuators is that they are zero-net-mass flux devices, i.e., they do not require fluid supply other than the ambient fluid of the exterior flow that is subject to AFC.

Often, the fluid flow occurs around a structural component that behaves as a 'bluff body', causing the flow to separate from its surface and a wake to be formed behind the body. Flow separation typically comes with the penalties of increased aerodynamic drag and less aerodynamic lift, thus a need to control these flows emerges. Examples of bluff-body flows include cross-flow over tubes, pipelines, cables, aerofoils, and turbine blades at high effective angles of attack, vehicles, etc. In addition, separated flows quickly become unstable and this is usually the case for Reynolds numbers encountered in practical applications. Important fluid-dynamical characteristics, such as mean and fluctuating fluid forces acting on the body, the energy transfer between flow and structure, etc., depend on the unsteadiness of the exterior flow. Thus, in order to bring about net improvements in performance, efficiency, and reliability, AFC methods have to exploit and/or modify the unstable nature of the exterior flow and change its global characteristics.

A previous review article which covers various passive and active control methods of bluff-body flows in both two- and three-dimensional configurations can be found in the work by the authors of [6]. In this review paper, we concentrate on AFC by plasma actuators, the perturbation fields caused by these actuators, and on recent results from the published literature with applications in nominally two-dimensional bluff-body flows. Because the flow around isolated circular cylinders has been extensively studied over a wide range of Reynolds numbers, it offers a convenient benchmark to compare the control authority of actuators at different operating conditions. This a selective review, so no claim of full coverage of the topic can be made.

2. Flow Control Definitions and Preliminary Remarks

A general introduction to flow control concepts and some preliminary remarks are required in order to acknowledge the plethora of different methods and the diversity of configurations. It is also important to appreciate the different AFC methods available in order to achieve a desirable flow, before selecting a particular one. Examples involving mostly bluff-body flows will be employed.

Flow control can generally be categorized into passive and active. Passive flow control does not require external supply of energy to work but relies on modifications of the shape or some other characteristic of the exterior surface of the body interacting with fluid flow. Helical strakes are often wrapped around long flexible pipelines that bring oil from the sea bottom so as to suppress unwanted flow-induced vibrations [7–9]. As an alternative to passively control the flow around a cylindrical structure, its surface can be fully or partially covered with hydrophobic or hairy-like microfiber coatings [10–12], or the geometry of the cylinder exterior be modified to have mild disturbances along its span [13,14].

In active flow control, external supply of energy is required to operate actuators that disturb the flow in steady or unsteady (usually periodic) mode [15]. For example, the flow characteristics around a cylinder in cross-flow can be modified by continuous windward suction and leeward blowing on the cylinder surface [16,17], by superimposing periodic pulsations on the exterior flow [18–20], or several other methods, for a more comprehensive list see the work by the authors of [6]. The benefits of AFC must be outweighed against the cost of implementing control, often in terms of energy efficiency.

Novel flow control concepts where energy is extracted from the exterior flow under control have been proposed, e.g., for controlling flow separation from a cascade of compressor blades [21]. In such a case, there will inevitably be some power and efficiency loss due to extracting part of the energy of the ambient flow. However, if the energy extracted from the exterior flow is a small percentage of the total kinetic energy of the flow, the effect of the actuators on the fluid flow mostly resembles one which would be achieved at the case energy, were externally supplied for the actuators to work.

AFC can be further divided into open-loop and closed-loop or feedback forcing. Strictly speaking a control system is closed-loop if a sensor is used to measure the effect of actuation on the system dynamics and the measured output is used to operate the actuator through a feedback loop. Hence, closed-loop control involves the interaction of sensors and actuators with the system dynamics coupled through predefined control laws, which govern the relationships between the sensor output and actuator forcing. In engineering, the subject dealing with control laws and their interaction with systems is system dynamics and control. Although classic control theory finds application in active closed-loop flow control, open-loop control is employed in the majority of AFC studies. A reason for this is that closed-loop control requires much more sophisticated hardware and software than open-loop control. Another reason is that basic control theory deals with linear or linearized system dynamics to facilitate analytical treatment [3]. On the other hand, most fluid flows are inherently nonlinear and it is generally more convenient to manipulate flows using open-loop control. In addition, the time lag between sensing and actuation introduced in the feedback loop can sometimes be a limiting factor.

With time, closed-loop flow control applications are gaining popularity but control parameters appear to be fuzzy [22–24]. An example with the cylinder wake flow will be given to illustrate a few important points. Muddada and Patnaik [24] employed two small rotating cylinders as actuators to suppress vortex shedding in two-dimensional wake flow behind a much larger cylinder. The control cylinders were attached symmetrically at the rear of the main cylinder and their rotation rate was controlled. To minimize the total variance between the flow state, which was measured by a series of sensors in the wake centerline, and the desired target state, set to a non-oscillating wake as a function of time (the objective function), they implemented a proportional control law. In the final controlled state, the actuator cylinders rotate at constant speed, which is tantamount to using open-loop control. Interestingly, Muddada and Patnaik demonstrated that energy expenditure can be optimized through 'nimble' control, i.e., periodically switching on and off the actuator; again, this control strategy is not effectively different than using open-loop control with frequency-modulated actuation. The above example illustrates that significant lessons regarding AFC of bluff-body flows can be learned from studies involving open-loop control to which we will restrict our attention here. This restriction by no way lessens the challenge but provides the opportunity to uncover complex interactions between actuators and unsteady fluid flows.

Another distinction of AFC methods is between global and local perturbation methods. In the former case, the perturbation in the relative velocity between the body surface and the oncoming free stream is 'uniform' throughout the flow. For nominally two-dimensional flows around a circular cylinder placed in a free stream, global perturbation methods include oscillations of the cylinder in-line with the free stream [25–29] or transverse to the free stream [30–34], rotational oscillations of the cylinder [35–38], combinations of these types of cylinder oscillations [39–42], and superposition of sound waves or fluid pulsations on the free stream [18,43–51]. In principle, imposing global perturbations provides a means to modify the process of vortex formation and the shedding frequency, as well as other flow characteristics shown in numerous related studies including those cited above. For the ranges of parameters governing the global perturbations for which flow characteristics can be significant altered, there is concomitant modification of the aerodynamic forces acting on the cylinder. However, global perturbations generally are not energy-efficient. On the other hand, actuators of small size relative to the characteristic length scale of the body, can be employed to induce localized velocity perturbations in order to achieve the desirable flow characteristics with minimal energy consumption.

In the next section, AFC-local actuators that operate in unsteady mode are presented and their main characteristics discussed.

3. AFC Local Actuators

Actuators play an important role in active flow control. A classification of actuators for aeronautical applications along with a discussion of actuator construction, design specifications, characteristics, and selection guidelines is given in the work by the authors of [5]. Typically, AFC actuators are positioned on, or extend from, the surface of the body interacting with the fluid flow being controlled. Actuators can be oscillating rods, flaps, protrusions, splitter plates, etc. that modify the exterior geometry of the body as a function of time. For instance, piezoelectric bending actuators have been used to drive flaps to manipulate the flow at the back of a nominally two-dimensional blunt trailing edge [52] and active Gurney flaps have been used to control the aerodynamic characteristics of wind turbine blades [53]. In these examples, dynamic shape modification is enabled via servo-mechanisms or microelectromechanical systems to actively control the exterior flow. For bluff-body (non-aerodynamic) flows, examples of active open-loop control via the moving-surface method include the dynamic radial deformation of the cross-sectional diameter of a circular cylinder [54,55] and the flapping splitter plate attached at the back of a circular cylinder [56]. A pertinent passive control mechanism of the flow around circular cylinders, which is worthy of being mentioned here, is the hinged splitter plate, which can flap due to the vortex shedding in the wake; the hinging location, length, and material properties of the splitter plate determine their dynamic deformation, and their proper selection provides a means to control the flow [57]. A variation of this configuration, with flexible splitter plates that are free to flap in a similar manner, has been employed as an energy-harvesting device [58]. So in this case, instead of spending energy to control the flow, the same can be achieved while extracting energy from the controlled flow.

A different type of actuators are those that introduce a local disturbance (perturbation field) to the exterior fluid field without altering the exterior shape of the solid body; for some applications this may be important. Local flow modification can be achieved via small slots (orifices) build into the wall through which fluid can be injected to the exterior flow and/or sucked into an interior cavity. Such devices are called fluidic actuators [5]. A particular class of fluidic actuators are the so-called synthetic jets, which do not require external supply of fluid, but work by entraining ambient fluid from the exterior (zero-net-mass flux) [59]. A synthetic jet is 'synthesized' by pulsing fluid in and out through an orifice connecting an interior cavity below the surface to the exterior flow (i.e., the cross-flow around a bluff body). As the fluid exits the orifice during ejection phase, the flow separates from the edge of the orifice forming a vortex ring (for round slots) or twin vortex sheets (for plane slots). The vortex ring (sheet) rolls up into a discrete vortex that is advected away into the exterior flow by its own induced velocity. During the suction phase, the formed vortex has moved away sufficiently and is thus unaffected by the ambient fluid that is drawn into the cavity. The main characteristic of synthetic jets is that they can impart linear momentum to the exterior flow without net mass injection across the orifice. As a consequence, the pulsed jet has a spatial distribution which is considerably different than that of a continuous jet issued from the same orifice and having the same time-averaged momentum flux [59].

Recently, researchers have designed plasma-induced synthetic jets or spark-jet actuators generated via an electrical arc/spark discharge inside a small cavity connected to the exterior flow through an orifice. These plasma synthetic jet actuators (PSJA) can produce high peak jet velocities above 300 m/s at frequencies up to 5 kHz with electromechanical efficiencies of 0.1–1%. These features make PSJA suitable for control of high-speed flows in aeronautical applications. The formation and evolution of plasma-induced synthetic jets depends on the electrical discharge parameters—mainly the duration and energy disposition of the discharge—as well as on other parameters of the cavity/orifice system, as is the same for conventional piston/diaphragm driven actuators. Apparently, the location of the electrodes inside the cavity also exerts a strong influence on the pulsed-jet characteristics and thereby on the authority of PSJAs for active flow control [60]. The practical disadvantages of PSJAs

are due to the high gas temperatures that can be reached within the cavity and the interference of electromagnetic fields [60]. A review of several practical issues related to PSJA design and integration, its characterization in quiescent flow, low-order analytical models, and numerical simulations of the induced synthetic jets as well as of some recent examples in AFC applications can be found in the work by the authors of [61].

Local flow perturbations can also be effected by fluidic oscillators, which are devices that emit a continuous but spatially oscillating jet when supplied with pressurized fluid, see the work by the authors of [62] for a more detailed description. Their advantage is that fluid oscillations are self-induced and self-sustained and no moving parts are required as they are driven by internal flow instabilities. Such devices can produce oscillations with frequencies from the order of a hertz up to several kilohertz, thereby spanning much of the frequency range of conventional and plasma-based synthetic-jet actuators. A historical review of the development and evolution of fluidic oscillators can be found in the work by the authors of [63]. Their control authority may be anticipated to be similar to other pulsed-jet actuators. However, fluidic oscillators are not zero-net-mass flux devices, and thus require continuous fluid supply.

A novel technology that emerged as an alternative to fluidic actuators at the end of the 1990s and is suitable for use in gas flows is to use dielectric barrier discharge (DBD) plasma [64–68]. The DBD plasma actuators can induce steady or unsteady jets tangential to the surface on which they are mounted causing a net flux of momentum to the exterior flow somewhat similar to the synthetic jet. A common characteristic is that both synthetic-jet and DBD plasma actuators are zero-net-mass flux devices. It is an immense task to thoroughly review all AFC methods, even if attention is restricted to zero-net-mass flux actuators. Here, we will focus on DBD plasma actuators that interact with the exterior flow by locally modifying the fluid velocities near the surface of the body in a controllable and predictable manner. For this category of actuators, a considerable number of applications in bluff-body flows has appeared in the published literature in recent years. In the remaining part of this section, the main characteristics of DBD plasma actuators are described.
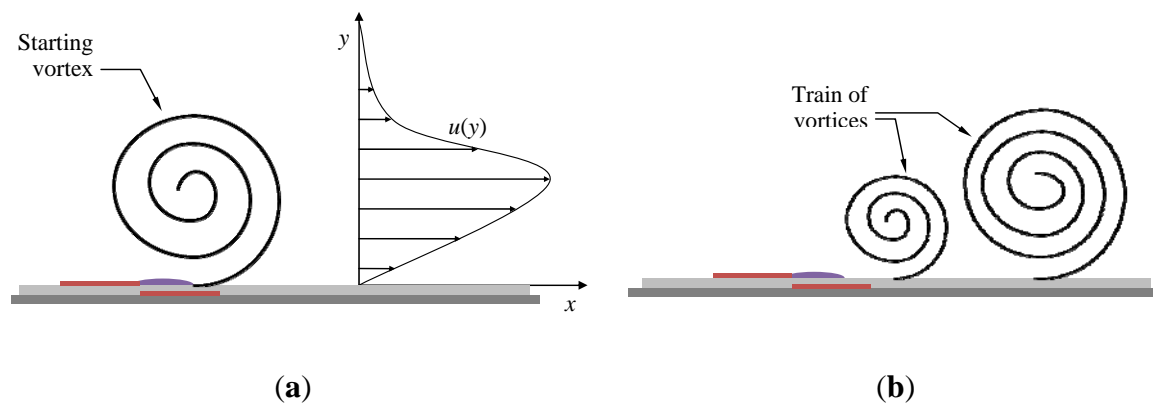
DBD Plasma Actuators

The basic configuration of a DBD plasma actuator is shown in Figure 1. It is composed of two electrodes separated by some dielectric material such as Teflon, Kapton, Plexiglas, ceramic, etc. The width of the electrodes typically is of the order of few millimetres. The one electrode is exposed and flush-mounted at the wall of the body where the flow is to be controlled. The other electrode is covered by the dielectric material and grounded. The electrodes are usually placed nonsymmetrically over both surfaces of the dielectric material with a small or no spacing between them. When high-voltage differential (of the order of kilovolts) is applied across the two electrodes, local ionization of the ambient air molecules over the exposed electrode occurs leading to the formation of nonthermal plasma. The formed plasma has a distinct purple-blue color. Ionized particles move from the exposed electrode towards the covered electrode inducing an air jet tangential to the wall called ionic wind or electric wind [69]. Collisions of the ionized species and ambient air produce a body force that acts as a momentum source and a flow control mechanism.
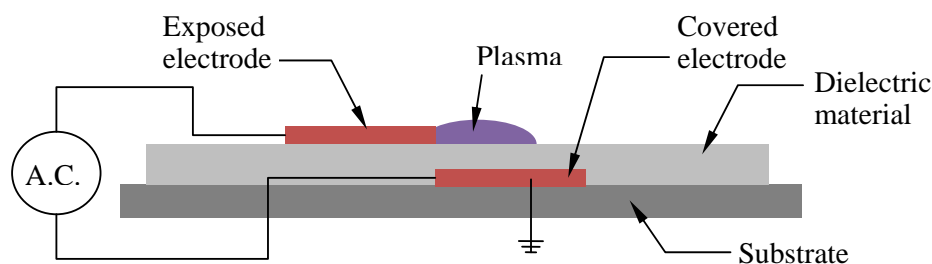
Figure 1. Schematic of the basic configuration of a dielectric barrier discharge (DBD) plasma actuator.

When the DBD electrodes are activated, a starting vortex is formed from the edge of the exposed electrode, as shown in Figure 2a. If the DBD is operated with high-frequency (of the order of kilohertz) alternating current (AC), the formed vortex develops with time and convects parallel to the wall towards the covered electrode. Thereby, the air surrounding the exposed electrode is entrained and a tangential wall jet is generated whose characteristics in quiescent air have been investigated in detail see, e.g., the work by the authors of [70]. DBD plasma actuators can also be operated in burst mode by periodically switching on and off the AC supply. In the burst mode, the plasma actuator induces the formation of a vortex in each burst leading to the formation of a train of co-rotating vortices, as shown in Figure 2b. These are starting vortices produced in each actuator burst. The ratio of time the actuator is turned on to the total time between consecutive turning on instants defines the duty cycle and effectively acts as the excitation frequency of the actuator. Operation of DBD plasma actuators in burst mode appears to be more effective and efficient than continuous operation [71–73]. The development of the starting vortex generated during continuous mode operation has been compared with the repeated vortices generated during burst mode operation using schlieren visualization and PIV [72].

(**a**)　　　　　　　　　　　　　　　　　　　　　　　　　　　　(**b**)

Figure 2. Flow induced by a single dielectric barrier discharge (DBD) plasma actuator operated in (**a**) continuous (steady) mode and (**b**) burst (unsteady) mode.

Figure 3 shows the development of the starting vortex in quiescent air from a DBD plasma actuator mounted on the surface of a circular cylinder from PIV [74]. The formation of starting vortices generated by DBD plasma actuators has similarities with the rolling up of the twin vortex sheets generated from the edges of the orifice in planar synthetic jets, however its orientation is tangential to the wall rather than normal. A major difference is that conventional planar synthetic jets generate equal amounts of positive and negative vorticity whereas DBD plasma generates preferential vorticity concentrations of a single sign. Different DBD electrode geometries can be employed to induce vortical structures with different topologies. For instance, two concentric annular electrodes, one exposed and the other one covered, can produce jets perpendicular to the wall [75]. In burst mode, a train of vortex rings can be generated with structure similar to that from synthetic-jet actuators.

The main advantages of DBD plasma actuators are that they can be easily installed on aerodynamic surfaces since they consist of solid-state electrical elements without moving parts, they can be mounted on flat and curved surfaces without introducing significant protrusions to the flow, they have low weight, they have tunable and fast time response, they have low power consumption and comparatively low cost, and are suitable for retrofitting on existing aerodynamic surfaces. A review of plasma actuator design for aerodynamic control techniques can be found in the work by the authors of [76]. Their major drawbacks of DBD plasma actuators are their high voltage requirement and their limitation in the perturbation velocity field reaching a maximum velocity of 7–8 m/s [77]. Another drawback that has not been widely reported is physical degradation after long use. The electrical and mechanical elements of plasma actuators have been thoroughly described in several review papers [4,78–80].
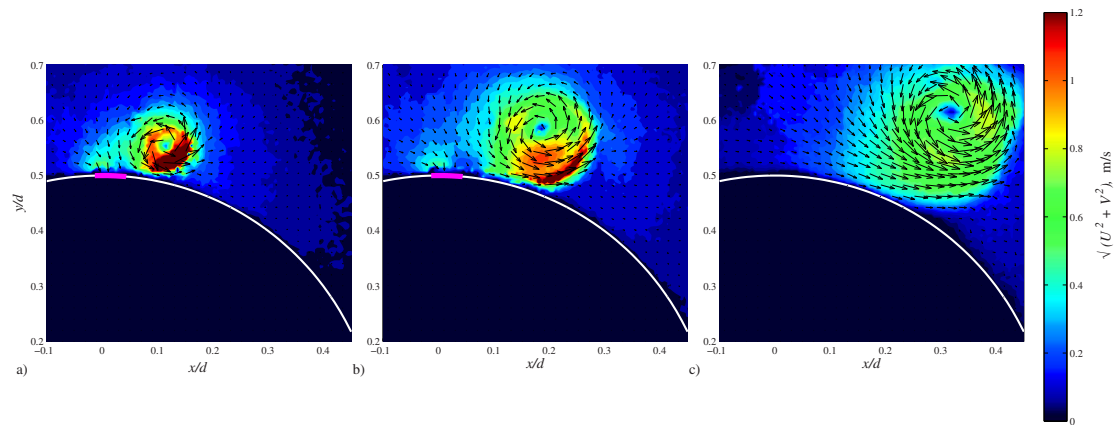
Figure 3. Development of starting vortex in quiescent air for a DBD plasma activated for 33 ms with AC at 25 kHz and ±3.5 kV. (**a**) 8 ms, (**b**) 24 ms, and (**c**) 56 ms after the plasma was fired. The plasma is schematically shown in pink color. Reprinted from the work by the authors of [74] with the permission of AIP Publishing.

Although the power consumption of DBD plasma actuators is low, i.e., low wattage, their electromechanical efficiency is of the order of 0.1% [81]. The electromechanical efficiency of DBD plasma actuators is defined as the ratio of mechanical power delivered to the air divided by the consumed electrical power to generate the plasma. A simple method to compute the mechanical power P_{mech} delivered to the surrounding atmospheric air, assuming that the plasma actuator induces a steady tangential wall jet with a homogeneous mean velocity profile $\overline{u}(y)$, is derived from the following relationship.

$$P_{mech} = \frac{1}{2} l_{act} \int_0^\infty \rho \overline{u}^3 \mathrm{d}y, \tag{1}$$

where l_{act} is the spanwise length of the actuator, $\overline{u}$ is the mean velocity component parallel to the wall, and y is the wall-normal direction. A more articulate computation of P_{mech} is from the body–force distribution $f_b(x, y)$ and the velocity field $u(x, y)$ in a two-dimensional domain surrounding the plasma actuator

$$P_{mech} = \iint\limits_{x,y} f_b(x, y) \, u(x, y) \, \mathrm{d}x \, \mathrm{d}y, \tag{2}$$

again assuming that distributions are homogeneous along the third direction. The body–force $f_b(x, y)$ or electrohydrodynamic (EHD) force acts as a momentum source term in the fluid motion equations, e.g., the Navier–Stokes equations for incompressible flows. The spatial distribution of the body force can be estimated by suitable lumped circuit models given the geometric design of electrodes and dielectric surface as well as electric discharge parameters [64,82,83] or from spatially-resolved measurements of the fluid velocity field [84,85]. Figure 4 shows the EHD force distribution from a typical DBD configuration as derived from PIV measurements of velocity field and from a theoretical model in the work by the authors of [85].

From the point of view of flow control, the characterization of the actuation strength of DBD plasma actuators poses a challenging task. The EHD force $f_b(x, y)$ and velocity $u(x, y)$ distributions vary with time as the alternating current. This is particularly important in low AC frequency and burst-mode operation of DBD actuators. Thus, the time-resolved measurements, phase-resolved measurements, or both measurements of the evolution of velocity perturbation fields in the neighborhood of the plasma are required to estimate the EHD force and the momentum imparted to the atmospheric air [64,83,86,87]. This is important for calibration and validation of numerical plasma models and also for setting appropriate realistic body–force distributions in CFD solvers.

In order to optimize the application of DBD plasma actuators for flow control, further studies of electric–wind, induced body force, and induced air momentum, and their relation to the

physical and electrical parameters of atmospheric plasmas, as well as their dependence on the operating environment (temperature, pressure, and humidity), are warranted. There are some pitfalls in characterization tests of DBD actuator mechanical performance associated with the accurate measurement of the induced electric wind [80]. The calculation ab initio of a dimensionless momentum coefficient, which can effectively characterize the actuation strength in terms of the induced body force, particularly in complex geometries, is essential to quantify fluid-dynamic effects and allow meaningful comparisons between studies employing different types of actuators.
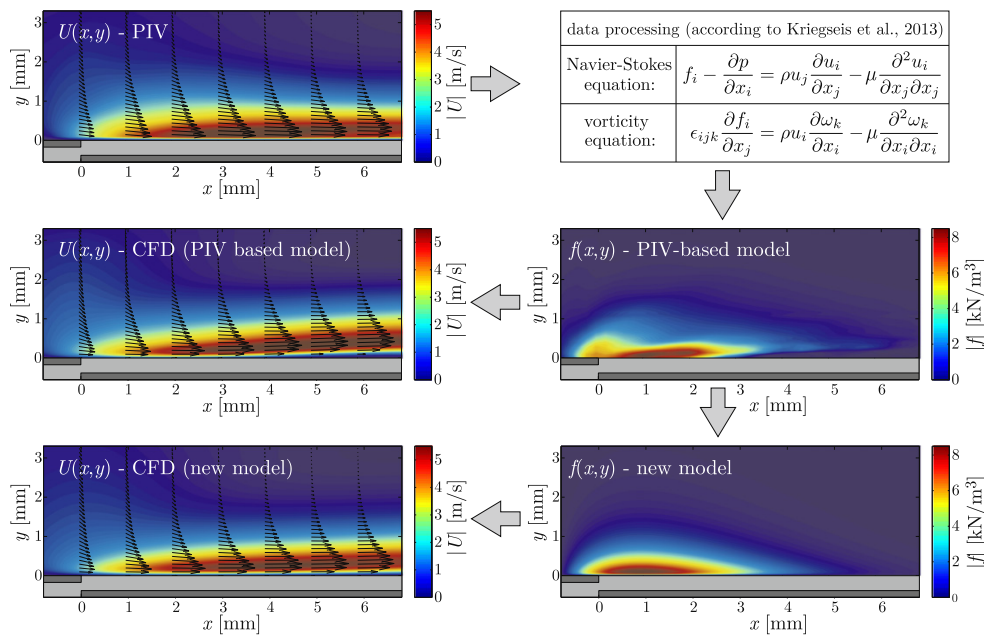
Figure 4. Electrohydrodynamic (EHD) force distribution derived from measurements of velocity field and from a theoretical model. Reprinted from the work by the authors of [85] with permission from Elsevier.

It is often useful to report a momentum coefficient C_μ which quantifies the momentum imparted to the fluid by the actuator compared to the momentum of the flow. The momentum coefficient is analogous to the one used for synthetic jets [59,88]. It can be estimated based on integrated momentum flux across velocity profiles normal to surface, i.e.,

$$C_\mu = \frac{\int_0^\infty \rho \overline{u}^2 \mathrm{d}y}{0.5 \rho_\infty U_\infty^2 D},$$

(3)

where U_∞ is the free-stream velocity and D is a characteristic length scale of the bluff body, e.g., the diameter of a circular cylinder. The air density ρ near the plasma may be spatially distributed due to thermal effects and slightly different than the bulk density of the exterior fluid ρ_∞, so this effect is taken into account in the above definition of C_μ.

Estimates of the maximum electric–wind velocity from knowledge of the electrical parameters through some empirical correlations would be useful but none seems to be available. Previous works show that the shape of the high-voltage active electrode and the length of the covered electrode influences the plasma physics, and thereby the EHD force distribution [64,87]. Generally, the electric–wind velocity increases with power consumption and AC voltage. It should also be noted that measurements of electric–wind velocity in the presence of cross flow may be different than those in quiescent air. It becomes evident that accurate estimation of the momentum coefficient is difficult. An alternative plasma force coefficient C_F, defined as

$$C_F = \frac{F_{ehd}}{0.5\rho U_\infty^2 D}, \tag{4}$$

can be also employed to characterize the strength of DBD plasma actuators. In the above expression F_{ehd} is the electrohydrodynamic force per electrode spanwise unit length, which is given by

$$F_{ehd} = \iint\limits_{x,y} f_b(x,y)\, \mathrm{d}x\, \mathrm{d}y. \tag{5}$$

The EHD force can be estimated from measurements of the induced velocity field or by direct force measurements on DBD surfaces [86,87]. The plasma force coefficient C_F represents the ratio of the actuator momentum to the free-stream momentum. Thus, it can be considered as equivalent to the momentum coefficient C_μ. Kotsonis et al. showed that ~30% of the electrically-induced momentum is consumed by wall friction, and thus does not contribute to the EHD-induced thrust on the dielectric surface. It should be noted that sometimes C_F is reported in place of C_μ in the published literature.

Modification of the input waveform that drives actuators provides a novel means to increase control authority, minimize power consumption, or both for achieving a specific control target. AFC experiments with synthetic jets have shown that varying the duration of blowing and suction periods changes the momentum coefficient, which therefore could be adjusted independently to some degree from the excitation frequency. Application on the flow around a circular cylinder demonstrated the efficacy of the varying blowing/suction method [89,90]. Small perturbations at multiple harmonic frequencies can have an impact on nonlinear interactions. For instance, nonharmonic perturbations have been found to modify the characteristics of vortex shedding in the wake and the aerodynamic forces on the cylinder [91].

An advantage of DBD plasma is that actuation is accomplished entirely by applying high-voltage AC to the electrodes. Thus, electronic circuits can be easily implemented to modify and/or modulate the AC input waveform. For instance, the influence of the input waveform of high-voltage AC on the DBD plasma morphology, the body force production, and time-dependent electric–wind have been studied experimentally in quiescent fluid [92]. Sine, square, sawtooth, and positive and negative ramp input waveforms were tested [92]. Such waveforms have a well-defined period (or frequency), although apparently the number and magnitude of harmonics required to represent each signal differs. Time-resolved measurements of EHD-induced velocities at selected points in the vicinity of the discharge showed that the flow response is quasi-linear with respect to the input electrical signal. The square waveform was found to be optimal in terms of mean body–force and mean electric–wind production but the sinusoidal waveform produced the highest velocity fluctuations.

Another means to modify the input waveform is by introducing amplitude or frequency modulations or by operating the actuator in burst mode, i.e., switching on and off the actuator for prescribed periods [93]. Again, electronic circuits can be readily implemented to generate the required input. Figure 5 shows examples of different input waveforms having the same carrier frequency, i.e, the main driving frequency of the actuator. These waveforms require at least two additional parameters to describe the level of modulation. For amplitude-modulated waveforms, a parameter quantifies the modulation frequency f_m and another the level of amplitude modulation, e.g., in the example shown, the waveform amplitude drops to zero in the middle of the period (see Figure 5). Note that amplitude modulation introduces a modulation frequency f_m. For burst-mode waveforms, a parameter is needed to describe the duration of each burst and another to describe the time interval between bursts. The latter parameter also introduces a modulation frequency f_m as indicated in the figure while the former parameter is usually is quantified by the duty cycle, which is defined as the ratio of burst duration to the time-interval between bursts.

Sinusoidal waveform

Amplitude modulated waveform

Burst modulated waveform

$$T_m = 1/f_m$$

Time
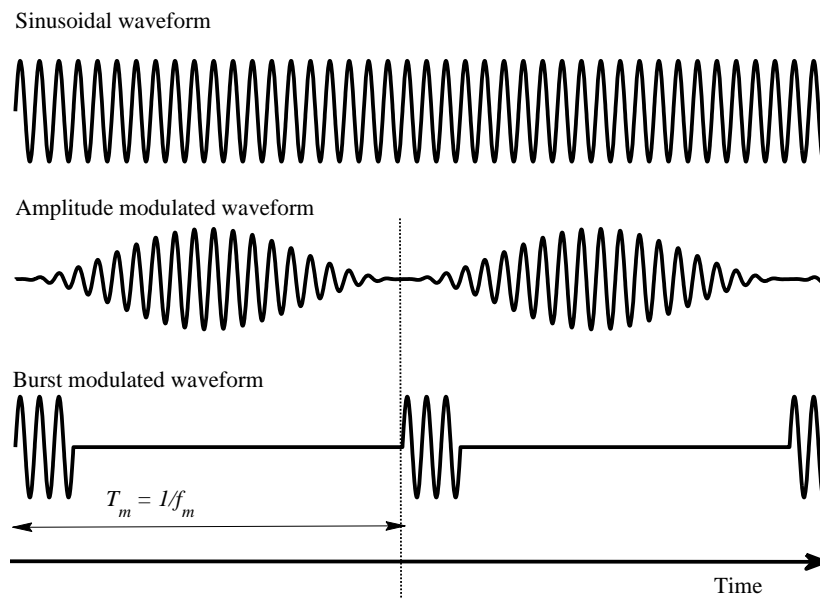
Figure 5. Different input waveforms having the same carrier frequency of the actuator. The definition of the modulation frequency f_m is also shown for modulated waveforms.

An appropriate dimensionless number to quantify the excitation frequency is the forcing Strouhal number St_f, which is defined as

$$St_f = \frac{f_e D}{U_\infty}. \tag{6}$$

It represents the ratio of the time scale of the exterior flow D/U_∞ to the time scale of the excitation $1/f_e$. Some caution is required in order to properly identify the excitation frequency. For AC activation of electrodes with sinusoidal input waveforms, f_e is the AC frequency. However, for amplitude-modulated or burst-modulated input waveforms, it is usually the lower modulation frequency, f_m, that acts as the excitation frequency, f_e. In the latter cases, it may be more relevant to take $f_e = f_m$.

For cross-flow over the exterior of bluff bodies, it is important to provide the necessary information regarding the momentum coefficient, C_μ, and the forcing Strouhal number, St_f, to facilitate the interpretation of results and comparisons between different studies. In addition, it is sometimes convenient to report the excitation frequency relative to the natural frequency of vortex shedding in the uncontrolled flow, which is the main global instability in bluff-body flows.

4. Fundamentals of Bluff-Body Flows—The Circular Cylinder

The flow around a circular cylinder has been an archetypal configuration in fluid dynamics which has been very extensively studied over a wide range of Reynolds numbers. For a circular cylinder of diameter D placed perpendicular to a free stream of uniform velocity U_∞ of a Newtonian fluid with density ρ and dynamic viscosity μ, the Reynolds number of this flow is defined as

$$Re_D = \frac{\rho D U_\infty}{\mu}. \tag{7}$$

The Reynolds number represents the ratio of inertial to viscous forces and its value determines the flow regime.

4.1. Stable Regime

For low Re_D values below 46–47, instabilities are suppressed by viscous effects, and the flow is steady and laminar everywhere. Such low Re_D values can be found in systems with very small

dimension and velocity or very large viscosity. For such systems, the size of actuators usually presents a significant constraint so real AFC applications are scarce.

4.2. Flow Instabilities

As the Re_D increases above the critical value of 46–47, a Hopf bifurcation trigers self-sustained wake oscillations, which can be predicted from linearized stability theory [94]. At Reynolds numbers slightly above the critical value, this instability leads to the formation of the famous von Kármán vortex street in the wake. It is important to note that although the nature of the instability is two-dimensional, vortex shedding remains in tact over a wide Re_D range from approximately 50 to 10^6 or even higher, i.e., this organized flow unsteadiness remains active well-inside the regime where three-dimensional turbulent flow occurs. For this reason, the study of the controlled flow around a circular cylinder at low-to-moderate Re_D values can provide some indication, rough at least if not good, of the control authority of different AFC methods at Reynolds numbers of practical interest. This is important for CFD methods which can be used with greater confidence at low Reynolds numbers.

The primary instability of the cylinder wake flow is characterized by periodicity, which is quantified by the Strouhal number, a dimensionless parameter defined as

$$St = \frac{f_{vs,0}D}{U_\infty}, \tag{8}$$

where f_{vs0} is the frequency at which vortices are shed from one side of the uncontrolled cylinder. AFC can modify the alternating mode of vortex shedding from each side of the cylinder, depending on the number and location of actuators as well as on actuation frequency and amplitude, to a different mode that may involve symmetrical shedding of vortices, or shedding of less or more vortices per actuation cycle, or even suppress the unsteadiness. In such cases, the reporting of the flow periodicities may require some care .

At $Re_D \approx 189$, secondary instabilities occur which lead to three-dimensional flow [95]. At higher Reynolds numbers, the instantaneous flow is three dimensional but the flow remains statistically homogeneous along the spanwise direction provided that sufficiently long circular cylinders are used and end effects are properly avoided in experiments. Tentatively, local AFC effects over a short central span of the cylinder can be considered as representative of that over the entire cylinder span, which should generally be checked in AFC experiments.

For Reynolds number up to 350–400, laminar three-dimensional vortex structures are shed from the cylinder and become turbulent downstream, i.e., transition to turbulence occurs in the wake [96]. At Re_D values higher than approximately 1000, Tollmien–Schlichting waves appear in the separated shear layers arising from Kelvin–Helmholtz instability, which causes a transition to turbulence. The frequency of the shear-layer instability, f_{sl}, scales with the frequency of vortex shedding in the wake f_{vs0} [97]. The possibility of resonance between the excitation frequency, f_e, of actuators and f_{sl} should be examined when interpreting results in relevant AFC studies.

4.3. Boundary Layer Transition

The point of transition to turbulence gradually moves upstream from the separating shear layers until it reaches the surface of the cylinder at $Re_D \approx 10^5 - 3.5 \times 10^5$. At higher Reynolds numbers, the boundary layer becomes transitional then fully turbulent. The boundary layer transition is associated with marked changes, i.e., separation is delayed after the apex of the cylinder, the vortex shedding frequency increases, and the aerodynamic drag decreases substantially (drag crisis). In this regime, the flow is sensitive to the roughness of the cylinder surface. Small roughness elements or protrusions can promote transition to turbulence. Consequently, the surface anomaly introduced by mounting actuators there can have a considerable effect on the flow even when the actuator is not activated. This has been observed in force-balance measurements on a circular cylinder for the baseline uncontrolled flow, i.e., with DBD plasma actuators mounted but not activated; the drag

coefficient decreases from approximately 1.07 at $Re_D = 6 \times 10^4$ to 0.87 at $Re_D = 10^5$ [98]. This indicates that the roughness introduced by the four electrodes that were flush-mounted on the cylinder surface caused premature transition in the boundary layers compared to the canonical flow over a smooth cylinder.

5. AFC Application on Flows Around Bluff Cylinders

In this section, we consider AFC applications of the flow around a circular cylinder by plasma actuators. Depending on the geometrical configuration of the electrodes producing the discharge, the actuation induce velocity perturbation fields (electric–wind) in close proximity to the actuators that may be symmetric or asymmetric with respect to the plane (or axis in 2D) of symmetry of the flow. In addition, symmetrically-located actuators can be operated in-phase or out-of-phase. In the case of antiphase forcing (i.e., 180° out-of-phase), an antisymmetric perturbation field is produced, which has the spatio-temporal symmetry of the original unsteady field associated with von Kármán vortex shedding. In the following, material is presented based primarily on the above classifications.

5.1. Symmetric Perturbations

5.1.1. Effect of Actuator Configuration

Most AFC studies consider the symmetric forcing of flow around a circular cylinder. An early study by Artana et al. demonstrated the capability of plasma actuators without dielectric barrier to control the cylinder wake [99]. A wire and a plate electrode were flush-mounted on the surface at the front and rear stagnation points of the cylinder, respectively, and were excited with DC to create a plasma sheet contouring the cylinder. The sheet produced was symmetric with respect to the flow symmetry axis, i.e., the axis parallel to the free stream passing through the cylinder center. Note that there is no dielectric barrier in this configuration. Figure 6 shows that activation of the EHD actuator resulted in the elimination of large-scale vortices in the wake of the cylinder. Surface pressure measurements showed that the EHD actuator caused mild changes in the pressure distribution around the cylinder and small increases in base pressure coefficient at the back stagnation point $-C_{pb}$ over a range of Reynolds numbers $2.3 \times 10^3 < Re_D < 5.8 \times 10^4$, indicating a less pronounced control effect on the flow than that inferred from visualization pictures (Figure 6).

Also, before the development of DBD plasma actuators, Hyun and Chun used ionic wind produced by locally ionized air from a corona discharge for AFC. They used an aluminum foil electrode, which covered the entire cylinder, and one or two stainless steel thin wires as discharge electrodes [100]. The discharge electrodes were mounted inside the flow with their axes parallel to the cylinder axis. When one discharge electrode was used it was placed along the symmetry axis, whereas when two discharge electrodes were used they were placed on symmetrical positions with respect to the symmetry axis. Hence, the flow symmetry was maintained in all cases. Several different configurations of the discharge electrodes were tested. Smoke visualization showed that the direction of the ionic wind can have a dramatic influence on the flow around the cylinder. For some electrode configurations, it was possible to channel the flow around the cylinder whereas the flow streamlines moved away from the cylinder for some other configurations. These flows were created by steady ionic winds which could be predicted by a physical model [100]. The disadvantage of this actuator configuration is that wires are not mounted on the cylinder surface but have to be placed inside the flow.

In order to achieve a similar effect, several single DBD actuators can be employed to channel the flow in the desired direction. Sung et al. placed six DBD plasma actuators at ±90°, ±120°, and ±150° from the front stagnation point [101]. The DBD electrodes were configured on the cylinder surface so as to impose a body force that is either along (forward configuration) or contra (backward configuration) to the free-stream direction. Figure 7 shows the effect of these configurations on flow patterns from smoke visualization. In the forward configuration, the flow remains attached to the rear side of the cylinder (Figure 7a). In the backward configuration, the flow appears to separate well before the apex

of the cylinder on the front side and a wide wake forms on the rear side (Figure 7b). In comparison, the uncontrolled flow separates just before the apex of the cylinder, while a small-scale eddy appears in the separating shear layer (Figure 7c).
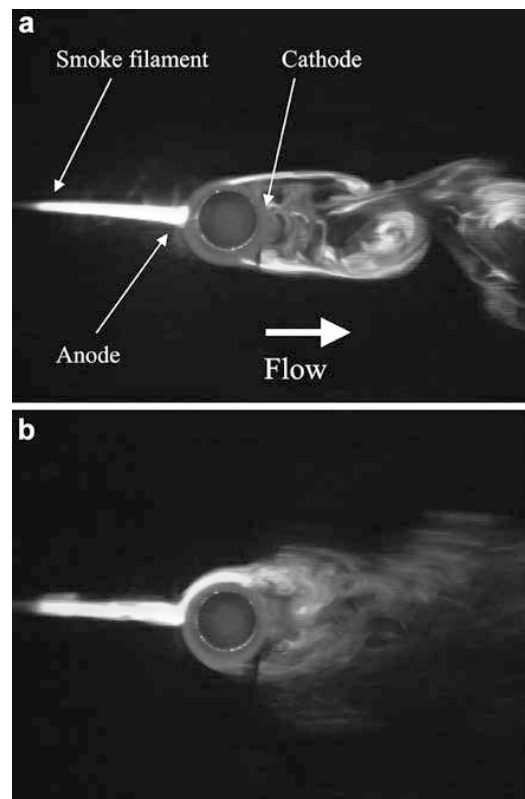

Figure 6. Smoke visualization of the instantaneous flow around a circular cylinder at $Re_D \approx 2.5 \times 10^3$ before (**a**) and after (**b**) a plasma actuator was activated. Reprinted by permission from the work by the authors of [99], © Springer-Verlag, 2003.

More recently, acoustic far-field measurements have shown that the contraflow configuration of two DBD plasma actuators at $\pm 85°$ from the front stagnation point are capable of reducing noise generation from a circular cylinder in cross-flow at $Re_D = (1.06 - 2.18) \times 10^5$ by 10 dB [102]. The effectiveness of DBD plasma actuation was established for actuator placement within $80° \leq |\theta_A| \leq 90°$ and for burst operation at $St_f > 1.5$. Threshold values exist for the electrical power fed to the actuators and the duty cycle of ~100 W and 25%, respectively. The wake width and turbulence levels behind the cylinder were both reduced in the contraflow (backward) configuration compared to the uncontrolled flow. These findings in the work by the authors of [102] seem to contrast the flow behavior in the earlier study by the authors of [101], both with contraflow configuration, but this is debatable as investigators employed different measurement techniques.

Alternative DBD plasma configurations can comprise three electrodes [103]. Figure 8 shows a particular three-electrode DBD (TEDBD) configuration mounted on a circular cylinder (note that this is not a sliding discharge [4]). When a positive DC component is applied to electrode 3; the induced electric–wind is similar to that with a two-electrode configuration, but the plasma-induced jet velocity increases with a marginal increase in power consumption. For instance, a jet velocity of 1.7 m/s could be obtained with TEDBD operated at AC voltage of 15 kV whereas the same velocity required AC voltage of 17 kV to be obtained with the regular DBD configuration. Drag measurements as a function of the momentum coefficient on a circular cylinder for Reynolds numbers of 8300 and 10,560 gave similar results for both the regular DBD and TEDBD configurations. This might indicate that the electric–wind characteristics are similar for both configurations but TEBDB can be used to increase the electric–wind.
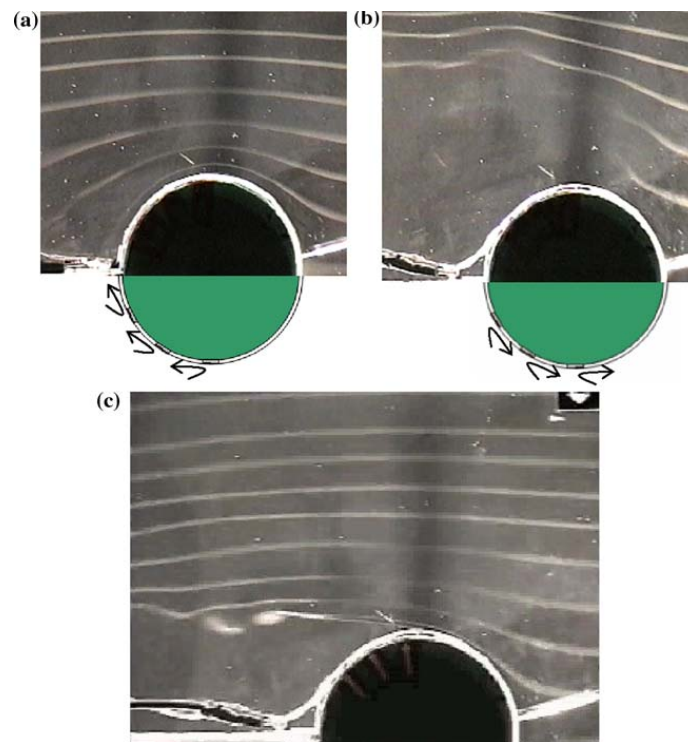
Figure 7. Smoke visualization of the instantaneous flow around a circular cylinder with and without DBD plasma actuators at $Re_D = 1.8 \times 10^4$: (**a**) Forward electrode configuration, (**b**) backward electrode configuration, and (**c**) uncontrolled flow. The free stream is from right to left and the schematics on the lower half of the pictures show the flow induced by the DBD actuators. Reprinted by permission from the work by the authors of [101], © Springer-Verlag, 2006.
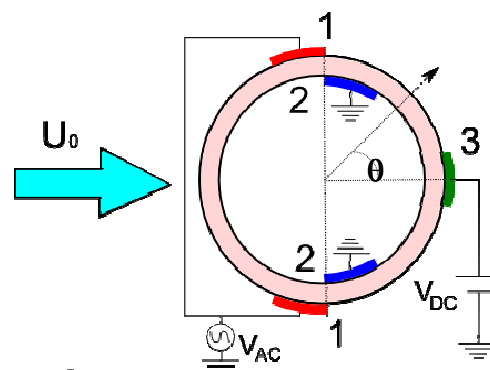
Figure 8. A DBD plasma actuator comprised of the three-electrode configuration. Numbers indicate the different electrodes (from the work by the authors of [103]). The arrow shows the free stream direction.

Recently, D'Adamo et al. used a modified three-electrode DBD configuration in which the exposed electrode covers the entire front side of the cylinder (from $-90°$ to $+90°$), the insulated electrode runs over the entire $360°$ inside the dielectric, and the third electrode is at the back stagnation point $180°$ [104]. With this arrangement and steady mode operation (9 kHz; 11 kV AC), the drag coefficient C_D could be reduced from ≈ 1.1 in the uncontrolled flow down to ≈ 0.80 with regular DBD actuation, which could be further reduced to ≈ 0.64 by DC energizing the third electrode (TEBDB) at the highest DC voltage of 11kV ($C_\mu = 0.15$). Remarkably, C_D could be further reduced to ≈ 0.56 by operating the actuators in the burst mode and selectively forcing at $f_e \approx f_{vs,0}$ ($St_f \approx 0.20$). A duty cycle of at least 31% was necessary to attain this amount of reduction. It should be noted that C_D was estimated from time-averaged mean velocity profiles in the wake obtained with a PIV system.

D'Adamo et al. argued that the significant drag reduction found for unsteady mode operation might be due to locking-on of the excitation and vortex shedding frequencies. However, other studies have shown that vortex lock-on is associated with amplification of the vortex shedding and increase of the aerodynamic drag as discussed below. The observed differences suggest that the geometry of the electrodes and their arrangement on the cylinder surface is of utmost importance.

More recently, Zhang et al. employed two symmetric DBD plasma actuators in a novel configuration such that plasma formed both upstream and downstream of the exposed electrodes [105]. The covered electrode run the entire circumference of the cylinder as in D'Adamo et al. but two short uncovered electrodes running from 88 to 92° were mounted on the exterior of the cylinder (angles measured from the front stagnation point). With this configuration, pairs of counter-rotating starting vortices were induced both upstream and downstream of the exposed electrodes, and produced rotating vortical structures on the surface. The effect resembles that produced by the action of rotating cylinders mounted symmetrically on the cylinder surface, so the method was termed as virtual moving surface boundary layer control. At $Re_D = \times 10^4$, the mean drag coefficient decreased with increasing the momentum coefficient by up to 25% at the highest C_μ value of 35%.

5.1.2. Effect of Excitation Frequency

Thomas et al. conducted a series of experiments using four single DBD plasma actuators to control flow separation and unsteady vortex shedding from a circular cylinder in cross-flow at $Re_D = 3.3 \times 10^4$ [106]. The exposed and covered electrodes of each actuator had no gap between them with their plasma-generating edges centered at $\pm 90°$ and $\pm 135°$. Care was taken to place the actuators sufficiently far apart so that plasma does not form between electrodes from individual actuators. They applied sinusoidal excitation to the electrodes ($\approx$ 11.5 kV at 10 kHz) in both steady and unsteady mode yielding $C_\mu = 1.1\%$ and 0.3%, respectively. In the unsteady operation mode (burst-modulated input), the bottom and top pairs of actuators were activated either in-phase (inducing symmetrical perturbations) or antiphase (inducing antisymmetrical perturbations). When actuators operated in steady mode, the extent of the separated flow region was substantially reduced and the von Kármán vortices appeared to be eliminated from the near wake, in agreement with previous studies with similar actuator configurations (e.g., the work by the authors of [101]). Unsteady forcing at $St_f = 1$, i.e., at approximately five times the frequency of vortex shedding in the uncontrolled flow, caused a reduction of the wake width and elimination of the von Kármán vortices for both in-phase and antiphase excitation. Further tests showed that duty cycle effects were small unless the duty cycle was reduced to 10%, in which case the flow control efficiency was compromised. When the actuators operated in unsteady synchronous mode (in-phase excitation) with the duty cycle fixed at 25%, plasma-induced symmetric perturbations at frequencies near the natural Strouhal frequency $St_f \approx St = 0.21$ caused vortex shedding to lock-on to the subharmonic of the excitation frequency f_m. The locking-on of vortex shedding to the subharmonic of the excitation frequency is tantamount to the effect of symmetric global perturbations of the free stream velocity [19,44,48,51,107] as well as of local symmetric perturbations induced by properly placed synthetic jets [108–110]. The subharmonic vortex lock-on occurs in a V-shaped region (Arnold tongue) in the parameter space of normalized amplitude and frequency, which theoretically originates at $f_e = 2f_{vs,0}$ at zero amplitude as shown in Figure 9.

It is useful to note that the required amplitude of localized velocity perturbation for symmetric DBD plasma actuators to cause subharmonic lock-on at $St_f = 0.21(f_e \approx f_{vs,0})$ and $Re_D = 3.3 \times 10^4$ in the work by the authors of [106] is estimated here to be of the order of the free-stream velocity. This can be compared to the corresponding amplitude of velocity perturbations of the free stream of $0.52U_\infty$ for the data-point at $f_e/f_{vs,0} = 1$ and $Re_D = 4 \times 10^4$ from Barbi et al. [51] in Figure 9 (note that $\Delta u/U_\infty = 2\pi\varepsilon St_f$). This demonstrates that the amplitude of localized velocity perturbations to cause lock-on is of the same order of magnitude as that for global flow perturbations. Note that the energy required to generate local perturbations is only a very small fraction of that required to produce global perturbations, which gives an indication of the energy efficiency of AFC by DBD plasma actuators.
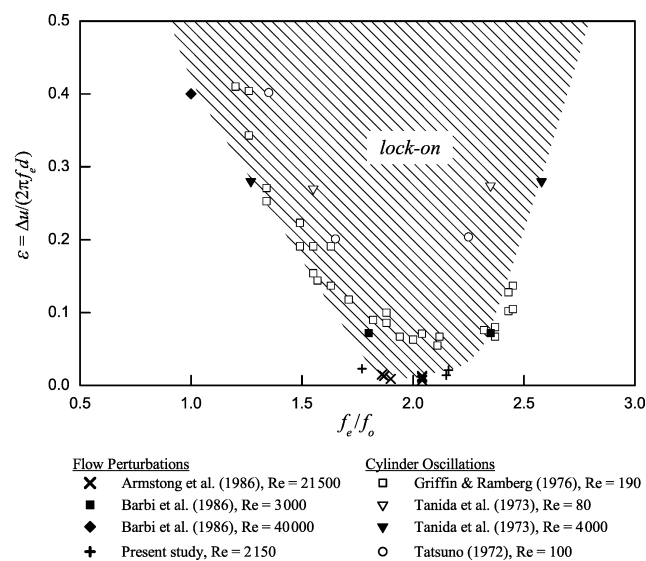
Figure 9. The subharmonic lock-on region of vortex shedding from a circular cylinder subjected to global symmetrical perturbations in-line with the free stream, i.e., perturbations of the free-stream velocity and streamwise cylinder oscillations. In the vertical axis label, Δu is the peak-to-peak amplitude of velocity perturbation, f_e is the excitation frequency, and d is the cylinder diameter, while in the horizontal axis, label f_o is the natural frequency of vortex shedding in the unperturbed flow. Reprinted from the work by the authors of [19] with permission from Elsevier.

In the work by the authors of [106], phase-locked PIV measurements revealed that a pair of symmetric vortices were generated in the very near wake of the cylinder during each actuation cycle for unsteady symmetric actuation ($St_f = 1$, duty cycle 25%). Again, this resembles the symmetric mode of vortex formation in the very near wake which can be attained by symmetric global perturbations of the free stream velocity [46,51] as well as by symmetric local perturbations induced by synthetic jets [108–110]. The symmetric mode typically occurs for high excitation frequencies, $f_e/f_{vs,0} > 3.0$. However, the symmetrically formed vortices move along a parallel path quite close to the wake centerline, possibly due to the vectoring of the flow on the rear side of the cylinder by the DBD plasma actuators. As we shall see immediately below, the symmetric formation of small-scale vortices in the separating shear layers provides an effective means to control the aerodynamic forces acting on the cylinder.

The efficacy of the symmetric mode to reduce mean drag and lift fluctuations was quantified at $Re_D = 1.5 \times 10^4$ by Jukes and Choi [111] . They used two DBD plasmas at $\pm 89°$ in the forward configuration. The exposed electrodes were supplied with AC with a square waveform at 33 kHz, ± 7 kV, and duty cycle 45%. The DBD actuators were operated in the pulse (burst) mode at nondimensional forcing frequencies $St_f = 0.1 - 2.0$ with duty cycle 1–40%. The force coefficient C_F was determined from PIV measurements in the plasma region in still air to be in the range $0.04\% < C_F < 0.39\%$. They also reported the peak velocity of the plasma jet to be $U_j/U_\infty = 0.30$. For $St_f > 0.6$, small-scale vortices form in the separated shear layers each time the plasma was fired; these vortices travel parallel to the free steam and decay in the downstream in a similar manner to the work by the authors of [106]. Merging between subsequent vortices in the near wake was observed at the higher excitation frequencies. Jukes and Choi called this the 'no shedding mode', but clearly the symmetrical vortices get detached from the boundary layer and are shed in the downstream. In this mode, the mean drag was reduced by up to 32% and the lift fluctuations by up to 72% at highest excitation amplitude and frequency ($St_f = 2.0$ and $C_F = 0.32\%$). For $0.3 < St_f < 0.6$, vortex shedding locked on to the subharmonic of the excitation frequency ($f_{vs,0} = \frac{1}{2}f_e$) while for $0.1 < St_f < 0.3$ vortex shedding locked on to the excitation frequency ($f_{vs,0} = f_e$). Interestingly, vortex shedding locked on the $2f_e$ at $St_f = 0.1$ (superharmonic lock-on). The forcing amplitude as quantified by C_F did not have a marked effect although clearly a minimum level of 0.045% was necessary to incite the symmetric (or no

shedding) mode and a lower level of 0.02% was necessary to incite vortex lock-on. The subharmonic, harmonic, and superharmonic lock-on regimes found by Jukes and Choi can be predicted on the basis of extended linear theory using simple rules of spatio-temporal symmetry [112]. On the basis of the theory, it may be anticipated that further lock-on regimes can be attained by changing the phase between actuators on the bottom and top sides of the cylinder as discussed in the following subsection.

5.1.3. Effect of Antisymmetric Perturbations

The term antisymmetric means that perturbations fields have a spatio-temporal symmetry as the baseline flow; hence, in such cases, the unsteady perturbation fields may couple with the original unsteady fields. It is apparent from the above discussions that flow unsteadiness in the wake of a cylinder and thereby the mean drag as well as the the drag and lift fluctuations can be increased by amplifying the natural spatio-temporal symmetry of the flow. Rotational oscillations of the cylinder at frequencies near the natural frequency of vortex shedding clearly demonstrate this amplification [35,36,38]. Similar amplification can be attained by firing in antiphase (i.e., 180° out of phase) plasma actuators that are mounted symmetrically on the surface of the cylinder. Indeed, one of the earliest studies on AFC around circular cylinders employed antiphase excitation too [113]. For excitation frequencies near the natural frequency of vortex shedding in the uncontrolled flow, the wake evidently locked on to the excitation frequency. Several tests at different forcing levels of forcing were done which resulted in a well-defined Arnold tongue in the map of normalized amplitude and frequency [113].

Thomas et al. also conducted some experiments where DBD plasma actuators mounted on the top side of the cylinder were activated in antiphase with those on the bottom side [106]. They found that when the plasma was excited antisymmetrically at high frequencies ($St_f = 1$), visualization pictures showed that a narrow wake formed behind the cylinder, and hot-wire anemometry showed that velocity fluctuations were considerably suppressed in the wake, as in the case of in-phase symmetric excitation. This is an important result because it illustrates that at high forcing frequencies the actuators interact primarily with the instability of the individual shear layers on each side rather than tamper with the global instability of the wake flow, thereby resulting in a narrow wake with suppressed vortex shedding activity and reduced drag. This effect is opposite to that seen for antisymmetric forcing at low frequencies [113].

5.1.4. Effect of Waveform Modulation

Benard and Moreau used sinusoidal as well as amplitude- and burst-modulated input waveforms to control the flow around a circular cylinder [77]. Two DBD plasma actuators were mounted on the front part of the cylinder facing the flow. The exposed electrodes covered the region $20° \leq |\theta_A| \leq 50°$, while the insulated electrodes covered the region $50° \leq |\theta_A| \leq 100°$, so that the common edges of the electrodes of each actuator were at $\pm 50°$. The actuators were operated in-phase. This configuration is quite different than those in other works in which the origin of the actuators is usually on the rear part of the cylinder or close to the separation point [101,106,111]. Benard and Moreau found that for sinusoidal excitation at frequencies corresponding to $0.25 \leq St_f \leq 2.5$, the mean drag was always increased. A distinct peak with a maximum increase of 14% occurred at $St_f = 0.8$, i.e., for excitation at approximately the fourth harmonic of the vortex shedding frequency in the uncontrolled flow. The drag increase was stabilized at $C_\mu \approx 7\%$ for $St_f > 1.5$. The drag increases observed by Benard and Moreau, particularly at high excitation frequencies, can be contrasted to drag reduction found in tests were actuators are located at the back side [101,106,111]. This illustrates the very important effect of the actuators' locations on control authority for bluff-body flows with large areas of separation. It is conjectured here that the mean electric–wind produced by DBD plasmas located at the front side directs the flow away from the surface as the flow approaches the apex of the cylinder. As a result, the flow may separate at a larger angle with respect to the free-stream direction causing a wider wake to be formed behind the cylinder. Evidence for this can be seen in the distributions of the time-averaged Reynolds stresses which clearly show a wider wake (see Figure 12 in the work by the authors of [77]).

Interestingly, amplitude- and burst-modulated excitation had a marked effect on the aerodynamic drag compared to sinusoidal excitation [77]. Both types of input waveform caused the drag to increase, but distinct peaks now occurred at $St_f = 0.1$, 0.2, and 0.38, which approximately correspond to the first subharmonic and the harmonic and first-superharmonic of the natural vortex shedding frequency, due to vortex locking-on. The maximum percent increases in the drag coefficient were 30% for amplitude-modulated excitation and 27% for burst-modulated excitation; both cases at $St_f \approx 0.38$ (note that this is twice the maximum percent increase for sinusoidal excitation). Benard and Moreau also investigated the effect of the duty cycle for burst modulation and of the modulation index for amplitude modulation. Both parameters were found to have considerable influence. For instance, the percent increase in drag could drop from 30 to 10% by changing the duty cycle from 50% to 80% for forcing at the optimum frequency $St_f = 0.38$.

The results of Benard and Moreau clearly illustrate the coupling between periodic plasma excitation and the unsteadiness of the flow around a circular cylinder. We can see that in Figure 10, which shows distributions of phase-averaged vorticity around the cylinder for some of the test cases [77]. It should be noted that phase averaging was done by using the proper orthogonal decomposition method on PIV data [114–116] (i.e., measurements are not phase-locked with respect to the actuation). Interestingly, the peak vorticity in the center of the vortices seems higher in the baseline flow compared to the controlled flows. However, the vortices form much closer to the back of the cylinder while they are more compact in the controlled flows due to the lock-on phenomenon. These effects are more pronounced for locking-on at the subharmonic of the excitation frequency $\frac{1}{2}f_e$ when $St_f = 0.38$ (Figure 10c), than for locking-on at $\frac{1}{4}f_e$ when $St_f = 0.75$ (Figure 10b). These results are consistent with drag measurements, which showed a large increase in the controlled flows.
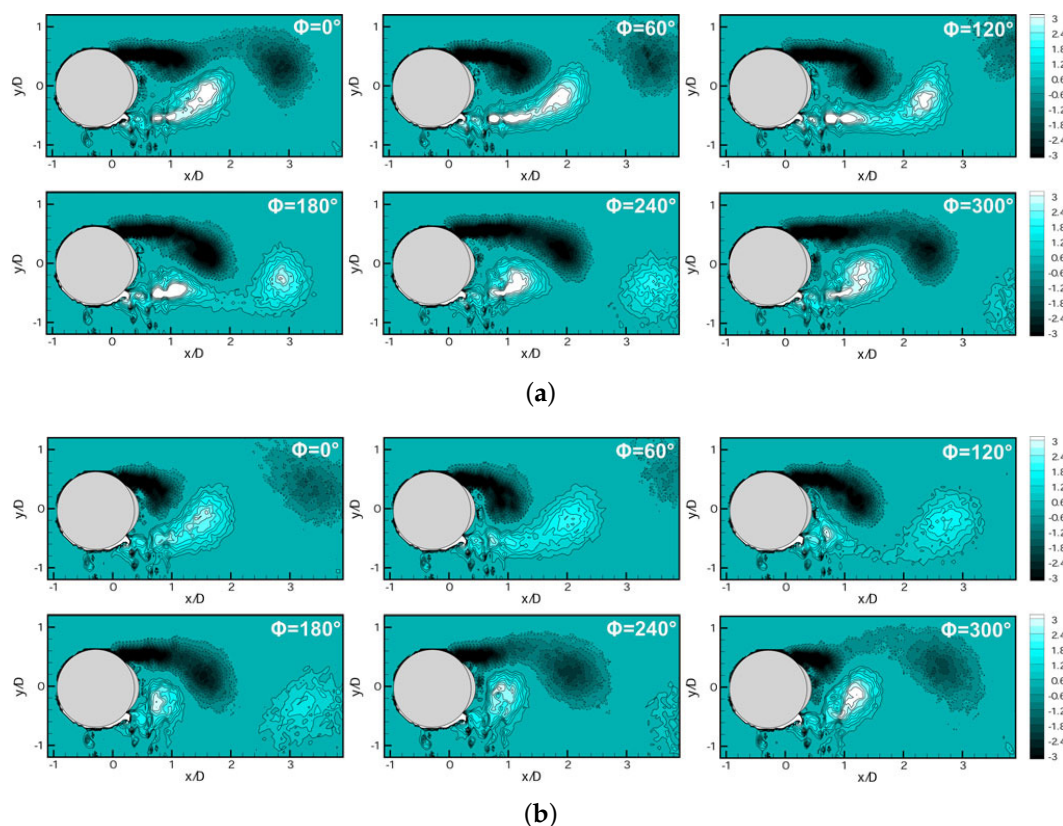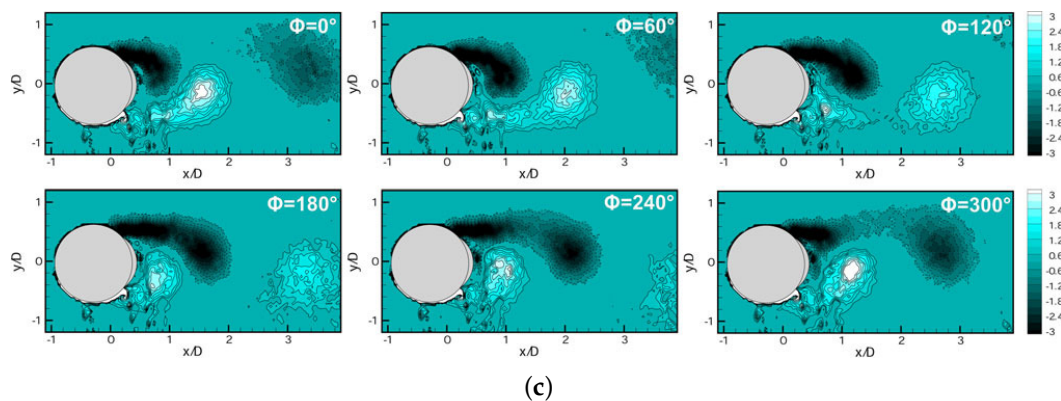

(a)

(b)

Figure 10. *Cont.*

(**c**)

Figure 10. Phase-averaged vorticity distributions around a circular cylinder at $Re_D = 4 \times 10^4$ with two DBD plasma actuators centered at $\pm 50°$. (**a**) Baseline flow with actuator turned off; (**b**) sinusoidal excitation at 300 Hz ($St_f = 0.75$); (**c**) amplitude-modulated excitation at $f_m = 150$ Hz ($St_f = 0.375$). The operating parameters of actuators in (**b**) and (**c**) correspond to the optimum for drag increase. Reprinted by permission from the work by the authors of [77], © Springer-Verlag, 2013.

5.2. Asymmetric Perturbations

Actuator configurations that create asymmetric perturbations to the flow have been studied, perhaps surprisingly, to much lesser extent than those which create symmetric or antisymmetric perturbations. The author is aware of only two studies where asymmetric forcing was employed; in one case, conventional steady and unsteady periodic forcing was used; whereas, in the other case, pulse-forcing was used to produce a transient response.

5.2.1. Continuous and Periodic Excitation

A very well-known example of mean lift generation is when a circular cylinder rotates around its center at constant speed. The addition of circulation of one sign causes the Magnus effect due to the no-slip condition and a mean force perpendicular to the free stream direction and the cylinder axis is generated. In an effort to replicate the Magnus effect, Sosa et al. mounted four electrode pairs, each producing DBD plasma, on a circular cylinder so as to create an electric–wind around the cylinder with a counterclockwise direction [98]. Direct measurements of the cylinder forces with an aerodynamic balance verified that mean lift can indeed be generated with this arrangement but the drag also increased. For steady mode operation, a mean lift coefficient of 0.05 was attained at $Re_D = 1.1 \times 10^5$. The mean lift coefficient was inversely proportional to the Reynolds number as expected from the classical Magnus effect ($\overline{C}_L \sim Re_D^{-1}$). They also found that burst-modulated excitation at frequencies close to the natural frequency of vortex shedding had more pronounced effects than forcing at other frequencies, possibly due to locking-on of the vortex shedding to the excitation frequency. A maximum value of the mean lift coefficient of 0.07 was attained for forcing at $f_e \approx f_{vs,0}$ at $Re_D = 1.1 \times 10^5$. For these parameters, the mean drag increased by up to 15%. The results indicate that the main effect of DBD plasma is due to the mean electric–wind that forces air near the surface to move tangentially in the counterclockwise direction.

5.2.2. Transient Perturbations

Jukes and Choi conducted a seminal experiment to investigate the capabilities of DBD plasma actuators for controlling unsteady flow separation from a circular cylinder in cross-flow [74]. For this purpose, they studied the effect of a short-duration burst of a single DBD plasma mounted on one side of the cylinder. This type of excitation causes an asymmetric but transient perturbation to the exterior flow. Figure 11 shows the effect of actuator location on the aerodynamic response of the cylinder. When the actuator was placed at $65° < \theta_A < 95°$, large increases in both drag and lift coefficients were observed for some time after the plasma burst, i.e., after ~$0.5T_K$. The flow was

reinstated at its original state after approximately eight vortex shedding cycles ($8T_K$) during which period the drag and lift fluctuations as well as the short-time-averaged mean drag remained higher than in the natural flow. The burst duration had only a minor effect on the aerodynamic response within the range of parameters investigated. On the other hand, the actuator location had considerable influence as can be seen in Figure 11. At $\theta_A = 60°$ and $100°$, the actuator is sufficiently away from the nominal separation point ($\theta_s = 82°$) to be capable of controlling the flow. The optimum plasma location for causing the largest changes to the aerodynamic forces was at $\theta_A = 75°$, i.e., just upstream of the nominal separation point.
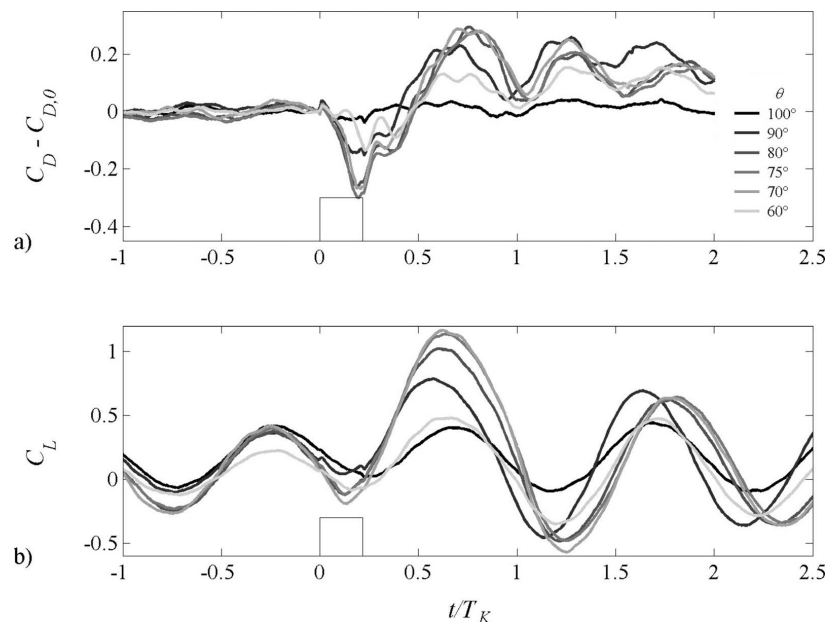
**Figure 11.** Time evolution of phase-averaged drag coefficient C_D (**a**) and lift coefficient C_L (**b**) acting on a circular cylinder subjected to short-duration excitation from a single DBD-plasma actuator mounted at different azimuthal locations on the cylinder surface; $Re_D = 1.5 \times 10^4$, $C_F = 0.45\%$. $C_{D,0}$, and T_K, respectively are the drag coefficient and the period of vortex shedding of the uncontrolled flow. The pulse duration ($0.22T_K$) is indicated on the figure by a rectangle. Reprinted from the work by the authors of [74] with the permission of AIP Publishing.

Jukes and Choi found that the pulse timing t_0 with respect to the phase of vortex shedding had a remarkable effect on both aerodynamic and wake response [117]. The phase of vortex shedding was obtained from the variation of the lift oscillations with the maximum taken as the time origin $t_0 = 0$. Figure 12 illustrates the effect of pulse timing t_0 on aerodyhanmic forces from which the wake response may also be inferred. For pulse timings in the range $0.1 \leq t_0/T_K \leq 0.6$, the plasma burst resulted in considerable increases in the aerodynamic forces. In these cases, a secondary vortex induced by plasma firing imparted its vorticity to a newly-forming vortex from the side of the actuator and increased the strength of the latter; thereby, vortex shedding became more vigorous and drag and lift fluctuations as well as the mean drag increased for 4–5 nominal periods of vortex shedding. On the other hand, the optimum pulse timing for reducing the aerodynamic forces is at $t_0/T_K = 0.875$, which corresponds to the case shown in Figure 13.

Figure 13 shows the basic mechanism of interaction between plasma excitation and the exterior flow from PIV [117]. This involves, initially, the break up of the connection between the boundary layer and the separated shear layer due to the momentum burst when the plasma is fired. This is followed by the formation of a secondary vortex after the burst, which is indicated by an arrow within the flow region in Figure 13c. The formation of the secondary vortex was strongly related to the pulse timing but was not related to the timing of vortex shedding. However, depending on the timing of

the pulse with respect to vortex shedding, the secondary vortex may disrupt the regular process of vortex shedding. In this case, the wake becomes nearly symmetrical and the shear layers become parallel to the free-stream without much interaction as seen in Figure 13d. This resulted in considerable decrease in the drag and lift fluctuations as well as in the short-time-averaged mean drag.
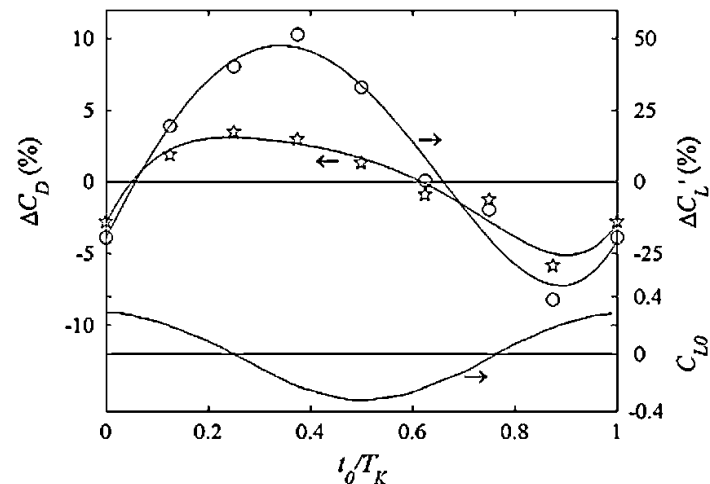
Figure 12. Changes in the mean drag and lift fluctuations averaged over $8.5T_K$ after plasma actuation as a function of the pulse timing for a circular cylinder subjected to short-duration ($0.05T_K$) excitation from a single DBD-plasma actuator mounted at $\theta_A = 75°$; $Re_D = 1.5 \times 10^4$. t_0/T_K represents the pulse timing with respect to the maximum in fluctuating lift $C_{L,0}$ when the plasma fires. Reprinted figure with permission from the work by the authors of [117]. Copyright by the American Physical Society, 2009.
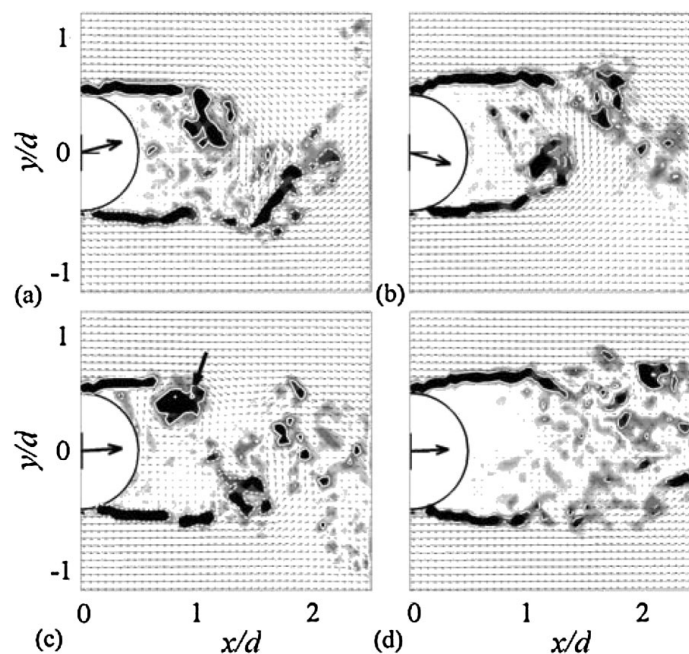
Figure 13. Instantaneous force vector acting on a cylinder and vorticity distributions around the cylinder subjected to short-duration ($0.05T_K$) excitation from a single DBD-plasma actuator mounted at $\theta_A = 75°$; $Re_D = 1.5 \times 10^4$, $C_F = 0.45\%$. (**a**) $t/T_K = -0.8$. (**b**) $t/T_K = -0.3$. (**c**) $t/T_K = 0.7$. (**d**) $t/T_K = 2.7$. In this case, the pulse timing $t_0/T_K = 0.875$ is optimum for reducing drag and lift fluctuations. Reprinted figure with permission from the work by the authors of [117]. Copyright by the American Physical Society, 2009.

The study of Jukes and Choi clearly illustrates the nonlinear interaction between DBD plasma pulse excitation and the unsteady exterior flow around a circular cylinder [74,117]. The injection of vorticity due to plasma firing can amplify or destruct the vorticity in the separated shear layer depending on the pulse timing with concomitant effects on aerodynamic forces.

6. Discussion

Several mechanisms of interaction between localized unsteady flow perturbations induced by plasma actuators and the inherently unsteady flow around bluff bodies can be predicted on the basis of similar mechanisms that have been observed for global flow perturbations. In particular, the effects of symmetric perturbations induced by unsteady plasma formation are analogous to the effects of global perturbations parallel to the exterior flow direction, e.g., the superposition of sounds waves and fluid pulsations on the free stream. This analogy concerns both the modes of vortex formation and frequency selection in the the wake of circular cylinders. For instance, it is now well acknowledged that with the increasing amplitude of global symmetric perturbations, these will eventually dominate over a large portion of the flow domain around a circular cylinder, thereby suppressing lift fluctuations [27,43,46,118,119]. Similar effects have also been observed with symmetric local forcing by a single synthetic jet located at either the front or back stagnation point, or a pair of symmetrically placed synthetic jet operated in-phase [89,108,112,120–123]. Similarly, locking-on of antisymmetric vortex shedding at the subharmonic of the excitation frequency, which is well known for global perturbations [19,43,44,51,107], has also been observed for symmetric in-phase excitation by plasma actuators.

It has been recently shown that modes of vortex formation can be interpreted in terms of generation of vorticity on the surface of the cylinder [107]. Forced global perturbations generate additional vorticity due to the induced relative motion between the flow and the cylinder surface. Although the net amount of additional vorticity is zero, due to contributions of both positive and negative vorticity, the phasing at which extra vorticity is introduced into the exterior flow determines the mode of vortex formation and the amount of vorticity that survives in the wake. Vorticity transport by diffusion and convection governs these complex processes, which involves cross-annihilation of oppositely signed vorticity. DBD plasma actuators by default induce perturbations with preferential vorticity concentrations as shown in Figure 3. Therefore, unsteady local injection of single-signed vorticity seems to be a mechanism that determines the control efficacy of DBD plasma actuators.

In addition to the above unsteady interactions, the electric–wind induced by DBD plasma exerts an additional control effect, which also plays a very important role in directing the flow around the cylinder or causing the flow to separate at large angles from the cylinder surface. These effects depend strongly on the geometry of the DBD electrodes and their placement on the surface of the cylinder. As a consequence, different studies with seemingly similar forcing have resulted in quite different results depending on the arrangement of the plasma actuators. This effect seems to overwhelm that due to the unsteady interactions discussed above.

7. Conclusions

The significance of actuator technology for active flow control will undoubtedly continue as AFC can yield considerable improvements in energy efficiency in numerous applications. This review aimed at providing a selection of information on the fluid-mechanical effects of plasma actuators for active control of bluff-body flows, which are characterized by flow separation and unsteadiness associated with large-scale as well as small-scale vortex structures. In terms of AFC application in bluff-body flows, the challenge is to find regimes where AFC operation can be well predicted and is thus safe. For the circular cylinder in particular, the promotion of symmetrical wake structures has been shown to be an effective means to suppress lift fluctuations and simultaneously decrease the mean drag. Conversely, unsteady excitation at frequencies sympathetic to the natural frequency of vortex shedding can cause vortex lock-on, which generally activates the wake flow and increases the

aerodynamic forces. Main actuator design specifications to achieve a desired control can be selected on the basis of the defined dimensionless parameters and results from several earlier studies presented in this paper.

From the point of view of plasma actuator technology, the dependence of performance characteristics on design parameters entails that further work must continue. The geometry and placement of the DBD electrodes, the amplitude and frequency of excitation, the input waveform, as well as the phase difference between individual actuators are key design parameters. A main challenge is to construct plasma actuators that can deliver high momentum coefficients which sets a practical limit of application to low-to-moderate flow speeds, given that the magnitude of induced velocity perturbations required to achieve effective control is often of the order of the free stream velocity. The power requirement of DBD plasma actuators is generally low but input waveform modulation can be used to optimize their low electromechanical efficiency. Another challenge is optimizing the perturbation fields, which provide the greatest control authority at a given power level. Our observations from consideration of bluff-body flows indicate that preferential vorticity concentrations within the induced plasma jets seem to offer a mechanism for more effective flow control. More research could be directed in designing novel actuators that can deliver these preferential vorticity concentrations. Experimental studies and modeling of different plasma actuators in quiescent fluid are important in order to link design/construction parameters (electrical circuit, actuator geometry, etc.) to the characteristics of the perturbation fields by plasma actuators, in order to minimize power requirements. The flow around a circular cylinder will continue to offer a convenient benchmark to compare the performance of different plasma actuators but also between different types of actuators in general.

Conflicts of Interest: The author declare no conflict of interest.

Abbreviations

The following abbreviations are used in this manuscript.

AC　　　Alternating Current
AFC　　　Active Flow Control
CFD　　　Computational Fluid Dynamics
DBD　　　Dielectirc Barrier Discharge
EHD　　　Electrohydrodynamic
PIV　　　Particle Image Velocimetry

References

1. Prandtl, L. Über Flüssigkeitsbewegung bei sehr kleiner Reibung. In Proceedings of the Third International Congress of Mathematicians, Heidelberg, Germany, 8–13 August 1904; pp. 484–491.
2. Gad-el-Hak, M. *Flow Control: Passive, Active, and Reactive Flow Management*; Cambridge University Press: Cambridge, UK, 2000.
3. Joslin, R.D.; Miller, D.N., Eds. *Fundamentals and Applications of Modern Flow Control*; American Institute of Aeronautics and Astronautics, Inc.: Reston, VA, USA, 2009; doi:10.2514/4.479892.
4. Corke, T.C.; Enloe, C.L.; Wilkinson, S.P. Dielectric Barrier Discharge Plasma Actuators for Flow Control. *Annu. Rev. Fluid Mech.* **2010**, *42*, 505–529. [CrossRef]
5. Cattafesta, L.N.; Sheplak, M. Actuators for Active Flow Control. *Annu. Rev. Fluid Mech.* **2011**, *43*, 247–272. [CrossRef]
6. Choi, H.; Jeon, W.P.; Kim, J. Control of Flow Over a Bluff Body. *Annu. Rev. Fluid Mech.* **2008**, *40*, 113–139. [CrossRef]
7. Quen, L.K.; Abu, A.; Kato, N.; Muhamad, P.; Sahekhaini, A.; Abdullah, H. Investigation on the effectiveness of helical strakes in suppressing VIV of flexible riser. *Appl. Ocean. Res.* **2014**, *44*, 82–91. [CrossRef]
8. Resvanis, T.; Rao, Z.; Vandiver, K. Effects of Strake Coverage and Marine Growth on Flexible Cylinder Vortex-Induced Vibrations. *J. Offshore Mech. Arct. Eng.* **2016**, *138*, 051801–051801-11. [CrossRef]

9.   Senga, H.; Larsen, C.M. Forced motion experiments using cylinders with helical strakes. *J. Fluids Struct.* **2017**, *68*, 279 – 294. [CrossRef]

10. Mastrokalos, M.E.; Papadopoulos, C.I.; Kaiktsis, L. Optimal stabilization of a flow past a partially hydrophobic circular cylinder. *Comput. Fluids* **2015**, *107*, 256–271. [CrossRef]

11. Huang, H.; Liu, M.; Gu, H.; Li, X.; Wu, X.; Sun, F. Effect of the slip length on the flow over a hydrophobic circular cylinder. *Fluid Dyn. Res.* **2018**, *50*, 025515. [CrossRef]

12. Hasegawa, M.; Sakaue, H. Microfiber Coating for Drag Reduction by Flocking Technology. *Coatings* **2018**, *8*. [CrossRef]

13. Tombazis, N.; Bearman, P.W. A study of three-dimensional aspects of vortex shedding from a bluff body with a mild geometric disturbance. *J. Fluid Mech.* **1997**, *330*, 85–112. [CrossRef]

14. Shi, X.D.; Feng, L.H. Control of flow around a circular cylinder by bleed near the separation points. *Exp. Fluids* **2015**, *56*, 214. [CrossRef]

15. De Giorgi, M.G.; De Luca, C.; Ficarella, A.; Marra, F. Comparison between synthetic jets and continuous jets for active flow control: Application on a NACA 0015 and a compressor stator cascade. *Aerosp. Sci. Technol.* **2015**, *43*, 256 – 280. [CrossRef]

16. Chen, W.L.; Li, H.; Hu, H. An experimental study on a suction flow control method to reduce the unsteadiness of the wind loads acting on a circular cylinder. *Exp. Fluids* **2014**, *55*, 1707. [CrossRef]

17. Gao, D.; Chen, G.; Chen, W.; Huang, Y.; Li, H. Active control of circular cylinder flow with windward suction and leeward blowing. *Exp. Fluids* **2019**, *60*, 26. [CrossRef]

18. Blevins, R.D. The effect of sound on vortex shedding from cylinders. *J. Fluid Mech.* **1985**, *161*, 217–237. [CrossRef]

19. Konstantinidis, E.; Balabani, S.; Yianneskis, M. The effect of flow perturbations on the near wake characteristics of a circular cylinder. *J. Fluids Struct.* **2003**, *18*, 367 – 386. [CrossRef]

20. Hong, S.; Huang, G.; Yang, Y.; Liu, Z. Introduction of DMD Method to Study the Dynamic Structures of a Three-Dimensional Centrifugal Compressor with and without Flow Control. *Energies* **2018**, *11*. [CrossRef]

21. Chen, J.; Lu, W.; Huang, G.; Zhu, J.; Wang, J. Research on Pulsed Jet Flow Control without External Energy in a Blade Cascade. *Energies* **2017**, *10*. [CrossRef]

22. Williams, J.F.; Zhao, B. The active control of vortex shedding. *J. Fluids Struct.* **1989**, *3*, 115 – 122. [CrossRef]

23. Roussopoulos, K. Feedback control of vortex shedding at low Reynolds numbers. *J. Fluid Mech.* **1993**, *248*, 267–296. [CrossRef]

24. Muddada, S.; Patnaik, B. An active flow control strategy for the suppression of vortex structures behind a circular cylinder. *Eur. J. Mech. Fluids* **2010**, *29*, 93–104. [CrossRef]

25. Leontini, J.S.; Lo Jacono, D.; Thompson, M.C. Wake states and frequency selection of a streamwise oscillating cylinder. *J. Fluid Mech.* **2013**, *730*, 162–192. [CrossRef]

26. Leontini, J.S.; Lo Jacono, D.; Thompson, M.C. A numerical study of an inline oscillating cylinder in a free stream. *J. Fluid Mech.* **2011**, *688*, 551–568. [CrossRef]

27. Marzouk, O.A.; Nayfeh, A.H. Reduction of the loads on a cylinder undergoing harmonic in-line motion. *Phys. Fluids* **2009**, *21*, 083103. [CrossRef]

28. Perdikaris, P.G.; Kaiktsis, L.; Triantafyllou, G.S. Chaos in a cylinder wake due to forcing at the Strouhal frequency. *Phys. Fluids* **2009**, *21*, 101705. [CrossRef]

29. Al-Mdallal, Q.; Lawrence, K.; Kocabiyik, S. Forced streamwise oscillations of a circular cylinder: Locked-on modes and resulting fluid forces. *J. Fluids Struct.* **2007**, *23*, 681 – 701. [CrossRef]

30. Anagnostopoulos, P. Numerical study of the flow past a cylinder excited transversely to the incident stream. Part 1: Lock-in zone, hydrodynamic forces and wake geometry. *J. Fluids Struct.* **2000**, *14*, 819 – 851. [CrossRef]

31. Leontini, J.S.; Stewart, B.E.; Thompson, M.C.; Hourigan, K. Wake state and energy transitions of an oscillating cylinder at low Reynolds number. *Phys. Fluids* **2006**, *18*, 067101. [CrossRef]

32. Carberry, J.; Sheridan, J.; Rockwell, D. Controlled oscillations of a cylinder: forces and wake modes. *J. Fluid Mech.* **2005**, *538*, 31–69. [CrossRef]

33. Williamson, C.; Roshko, A. Vortex formation in the wake of an oscillating cylinder. *J. Fluids Struct.* **1988**, *2*, 355 – 381. [CrossRef]

34. Ongoren, A.; Rockwell, D. Flow structure from an oscillating cylinder Part 1. Mechanisms of phase shift and recovery in the near wake. *J. Fluid Mech.* **1988**, *191*, 197–223. [CrossRef]

35. Kumar, S.; Lopez, C.; Probst, O.; Francisco, G.; Askari, D.; Yang, Y. Flow past a rotationally oscillating cylinder. *J. Fluid Mech.* **2013**, *735*, 307–346. [CrossRef]

36. Baek, S.J.; Sung, H.J. Quasi-periodicity in the wake of a rotationally oscillating cylinder. *J. Fluid Mech.* **2000**, *408*, 275–300. [CrossRef]

37. Baek, S.J.; Sung, H.J. Numerical simulation of the flow behind a rotary oscillating circular cylinder. *Phys. Fluids* **1998**, *10*, 869–876. [CrossRef]

38. Tokumaru, P.T.; Dimotakis, P.E. Rotary oscillation control of a cylinder wake. *J. Fluid Mech.* **1991**, *224*, 77–90. [CrossRef]

39. Jeon, D.; Gharib, M. On circular cylinders undergoing two-degree-of-freedom forced motions. *J. Fluids Struct.* **2001**, *15*, 533 – 541. [CrossRef]

40. Ongoren, A.; Rockwell, D. Flow structure from an oscillating cylinder Part 2. Mode competition in the near wake. *J. Fluid Mech.* **1988**, *191*, 225–245. [CrossRef]

41. Baranyi, L. Numerical simulation of flow around an orbiting cylinder at different ellipticity values. *J. Fluids Struct.* **2008**, *24*, 883 – 906. [CrossRef]

42. Nazarinia, M.; Lo Jacono, D.; Thompson, M.C.; Sheridan, J. Flow behind a cylinder forced by a combination of oscillatory translational and rotational motions. *Phys. Fluids* **2009**, *21*, 051701. [CrossRef]

43. Detemple-Laake, E.; Eckelmann, H. Phenomenology of Kármán vortex streets in oscillatory flow. *Exp. Fluids* **1989**, *7*, 217–227. [CrossRef]

44. Konstantinidis, E.; Liang, C. Dynamic response of a turbulent cylinder wake to sinusoidal inflow perturbations across the vortex lock-on range. *Phys. Fluids* **2011**, *23*, 075102. [CrossRef]

45. Kim, S.H.; Park, J.Y.; Park, N.; Bae, J.H.; Yoo, J.Y. Direct numerical simulation of vortex synchronization due to small perturbations. *J. Fluid Mech.* **2009**, *634*, 61–90. [CrossRef]

46. Konstantinidis, E.; Balabani, S. Symmetric vortex shedding in the near wake of a circular cylinder due to streamwise perturbations. *J. Fluids Struct.* **2007**, *23*, 1047 – 1063. [CrossRef]

47. Konstantinidis, E.; Balabani, S.; Yianneskis, M. Bimodal vortex shedding in a perturbed cylinder wake. *Phys. Fluids* **2007**, *19*, 011701. [CrossRef]

48. Konstantinidis, E.; Balabani, S.; Yianneskis, M. The timing of vortex shedding in a cylinder wake imposed by periodic inflow perturbations. *J. Fluid Mech.* **2005**, *543*, 45–55. [CrossRef]

49. Kim, W.; Yoo, J.Y.; Sung, J. Dynamics of vortex lock-on in a perturbed cylinder wake. *Phys. Fluids* **2006**, *18*, 074103. [CrossRef]

50. Meneghini, J.; Bearman, P. Numerical Simulation of High Amplitude Oscillatory Flow About a Circular Cylinder. *J. Fluids Struct.* **1995**, *9*, 435 – 455. [CrossRef]

51. Barbi, C.; Favier, D.P.; Maresca, C.A.; Telionis, D.P. Vortex shedding and lock-on of a circular cylinder in oscillatory flow. *J. Fluid Mech.* **1986**, *170*, 527–544. [CrossRef]

52. Gibeau, B.; Koch, C.R.; Ghaemi, S. Active control of vortex shedding from a blunt trailing edge using oscillating piezoelectric flaps. *Phys. Rev. Fluids* **2019**, *4*, 054704. [CrossRef]

53. Saenz-Aguirre, A.; Fernandez-Gamiz, U.; Zulueta, E.; Ulazia, A.; Martinez-Rico, J. Optimal Wind Turbine Operation by Artificial Neural Network-Based Active Gurney Flap Flow Control. *Sustainability* **2019**, *11*, 2809. [CrossRef]

54. Oualli, H.; Hanchi, S.; Bouabdellah, A.; Askovic, R.; Gad-El-Hak, M. Interaction between the near wake and the cross-section variation of a circular cylinder in uniform flow. *Exp. Fluids* **2008**, *44*, 807–818. [CrossRef]

55. Aissa, M.; Bouabdallah, A.; Oualli, H. Radial Deformation Frequency Effect on the Three-Dimensional Flow in the Cylinder Wake. *ASME J. Fluids Eng.* **2014**, *137*, 011104–011104-11. [CrossRef]

56. Wu, J.; Shu, C. Numerical study of flow characteristics behind a stationary circular cylinder with a flapping plate. *Phys. Fluids* **2011**, *23*, 073601. [CrossRef]

57. Shukla, S.; Govardhan, R.; Arakeri, J. Flow over a cylinder with a hinged-splitter plate. *J. Fluids Struct.* **2009**, *25*, 713–720. [CrossRef]

58. Akaydin, H.D.; Elvin, N.; Andreopoulos, Y. The performance of a self-excited fluidic energy harvester. *Smart Mater. Struct.* **2012**, *21*, 025007. [CrossRef]

59. Glezer, A.; Amitay, M. Synthetic Jets. *Annu. Rev. Fluid Mech.* **2002**, *34*, 503–529. [CrossRef]

60. Zhang, Z.; Wu, Y.; Jia, M.; Zong, H.; Cui, W.; Liang, H.; Li, Y. Influence of the discharge location on the performance of a three-electrode plasma synthetic jet actuator. *Sens. Actuators Phys.* **2015**, *235*, 71–79. [CrossRef]

61. Zong, H.; Chiatto, M.; Kotsonis, M.; De Luca, L. Plasma Synthetic Jet Actuators for Active Flow Control. *Actuators* **2018**, *7*. [CrossRef]

62. Woszidlo, R.; Ostermann, F.; Nayeri, C.N.; Paschereit, C.O. The time-resolved natural flow field of a fluidic oscillator. *Exp. Fluids* **2015**, *56*, 125. [CrossRef]

63. Gregory, J.; Tomac, M.N. A Review of Fluidic Oscillator Development. In Proceedings of the 43rd Fluid Dynamics Conference, San Diego, CA, USA, 24–27 June 2013. [CrossRef]

64. Corke, T.C.; Post, M.L.; Orlov, D.M. Single dielectric barrier discharge plasma enhanced aerodynamics: physics, modeling and applications. *Exp. Fluids* **2009**, *46*, 1–26. [CrossRef]

65. Thomas, F.O.; Corke, T.C.; Iqbal, M.; Kozlov, A.; Schatzman, D. Optimization of Dielectric Barrier Discharge Plasma Actuators for Active Aerodynamic Flow Control. *AIAA* **2009**, *47*, 2169–2178. [CrossRef]

66. De Giorgi, M.G.; Sciolti, A.; Campilongo, S.; Ficarella, A. Flame Structure and Chemiluminescence Emissions of Inverse Diffusion Flames under Sinusoidally Driven Plasma Discharges. *Energies* **2017**, *10*, 334. [CrossRef]

67. Pescini, E.; Marra, F.; De Giorgi, M.; Francioso, L.; Ficarella, A. Investigation of the boundary layer characteristics for assessing the DBD plasma actuator control of the separated flow at low Reynolds numbers. *Exp. Therm. Fluid Sci.* **2017**, *81*, 482–498. [CrossRef]

68. Pescini, E.; Martínez, D.; De Giorgi, M.; Ficarella, A. Characterization of the effects of a dielectric barrier discharge plasma actuator on a coaxial jet in a Bunsen burner. *Exp. Therm. Fluid Sci.* **2018**, *91*, 292–305. [CrossRef]

69. Robinson, M. A History of the Electric Wind. *Am. J. Phys.* **1962**, *30*, 366–372. [CrossRef]

70. Whalley, R.D.; Choi, K.S. The starting vortex in quiescent air induced by dielectric barrier discharge plasma. *J. Fluid Mech.* **2012**, *703*, 192–203. [CrossRef]

71. Greenblatt, D.; Wygnanski, I.J. The control of flow separation by periodic excitation. *Prog. Aerosp. Sci.* **2000**, *36*, 487 – 545. [CrossRef]

72. Mishra, B.K.; Panigrahi, P.K. Formation and characterization of the vortices generated by a DBD plasma actuator in burst mode. *Phys. Fluids* **2017**, *29*, 024104. [CrossRef]

73. Vernet, J.A.; Örlü, R.; Alfredsson, P.H. Flow separation control by dielectric barrier discharge plasma actuation via pulsed momentum injection. *AIP Adv.* **2018**, *8*, 075229. [CrossRef]

74. Jukes, T.N.; Choi, K.S. Flow control around a circular cylinder using pulsed dielectric barrier discharge surface plasma. *Phys. Fluids* **2009**, *21*, 084103. [CrossRef]

75. Santhanakrishnan, A.; Jacob, J.; Suzen, Y. Flow Control Using Plasma Actuators and Linear/Annular Plasma Synthetic Jet Actuators. In Proceedings of the 3rd AIAA Flow Control Conference, San Francisco, CA, USA, 5–8 June 2006. [CrossRef]

76. Wang, J.J.; Choi, K.S.; Feng, L.H.; Jukes, T.N.; Whalley, R.D. Recent developments in DBD plasma flow control. *Prog. Aerosp. Sci.* **2013**, *62*, 52–78. [CrossRef]

77. Benard, N.; Moreau, E. Response of a circular cylinder wake to a symmetric actuation by nonthermal plasma discharges. *Exp. Fluids* **2013**, *54*, 1467. [CrossRef]

78. Moreau, E. Airflow control by nonthermal plasma actuators. *J. Phys. Appl. Phys.* **2007**, *40*, 605–636. [CrossRef]

79. Kriegseis, J.; Möller, B.; Grundmann, S.; Tropea, C. Capacitance and power consumption quantification of dielectric barrier discharge (DBD) plasma actuators. *J. Electrost.* **2011**, *69*, 302–312. [CrossRef]

80. Kotsonis, M. Diagnostics for characterization of plasma actuators. *Meas. Sci. Technol.* **2015**, *26*, 092001. [CrossRef]

81. Benard, N.; Moreau, E. Electrical and mechanical characteristics of surface AC dielectric barrier discharge plasma actuators applied to airflow control. *Exp. Fluids* **2014**, *55*, 1846. [CrossRef]

82. Soloviev, V.R.; Krivtsov, V.M. Surface barrier discharge modelling for aerodynamic applications. *J. Phys. Appl. Phys.* **2009**, *42*, 125208. [CrossRef]

83. Mertz, B.; Corke, T. Single-dielectric barrier discharge plasma actuator modelling and validation. *J. Fluid Mech.* **2011**, *669*, 557–583. [CrossRef]

84. Kriegseis, J.; Schwarz, C.; Tropea, C.; Grundmann, S. Velocity-information-based force-term estimation of dielectric-barrier discharge plasma actuators. *J. Phys. Appl. Phys.* **2013**, *46*, 055202. [CrossRef]

85. Maden, I.; Maduta, R.; Kriegseis, J.; Jakirlić, S.; Schwarz, C.; Grundmann, S.; Tropea, C. Experimental and computational study of the flow induced by a plasma actuator. *Int. J. Heat Fluid Flow* **2013**, *41*, 80–89. [CrossRef]

86. Kotsonis, M.; Ghaemi, S.; Veldhuis, L.; Scarano, F. Measurement of the body force field of plasma actuators. *J. Phys. Appl. Phys.* **2011**, *44*, 045204. [CrossRef]

87. Debien, A.; Benard, N.; David, L.; Moreau, E. Unsteady aspect of the electrohydrodynamic force produced by surface dielectric barrier discharge actuators. *Appl. Phys. Lett.* **2012**, *100*, 013901. [CrossRef]

88. Cattafesta, L.N. Design of Synthetic Jets. In *Synthetic Jets: Fundamentals and Applications*; Mohseni, K., Mittal, R., Eds.; CRC Press: Boca Raton, FL, USA, 2015; pp. 49–97.

89. Feng, L.H.; Wang, J.J.; Pan, C. Effect of novel synthetic jet on wake vortex shedding modes of a circular cylinder. *J. Fluids Struct.* **2010**, *26*, 900 – 917. [CrossRef]

90. Feng, L.H.; Wang, J.J. The virtual aeroshaping enhancement by synthetic jets with variable suction and blowing cycles. *Phys. Fluids* **2014**, *26*, 014105. [CrossRef]

91. Konstantinidis, E.; Bouris, D. The effect of nonharmonic forcing on bluff-body aerodynamics at a low Reynolds number. *J. Wind. Eng. Ind. Aerodyn.* **2010**, *98*, 245–252. [CrossRef]

92. Benard, N.; Moreau, E. Role of the electric waveform supplying a dielectric barrier discharge plasma actuator. *Appl. Phys. Lett.* **2012**, *100*, 193503. [CrossRef]

93. Benard, N.; Moreau, E. Capabilities of the dielectric barrier discharge plasma actuator for multi-frequency excitations. *J. Phys. Appl. Phys.* **2010**, *43*, 145201. [CrossRef]

94. Triantafyllou, G.S.; Kupfer, K.; Bers, A. Absolute instabilities and self-sustained oscillations in the wake of circular cylinders. *Phys. Rev. Lett.* **1987**, *59*, 1914–1917. [CrossRef]

95. Williamson, C.H.K. Vortex Dynamics in the Cylinder Wake. *Annu. Rev. Fluid Mech.* **1996**, *28*, 477–539. [CrossRef]

96. Gerrard, J.H. The wakes of cylindrical bluff bodies at low Reynolds number. *Math. Phys. Sci.* **1978**, *288*, 351–382. [CrossRef]

97. Thompson, M.C.; Hourigan, K. The shear-layer instability of a circular cylinder wake. *Phys. Fluids* **2005**, *17*, 021702. [CrossRef]

98. Sosa, R.; Artana, G.; Benard, N.; Moreau, E. Mean lift generation on cylinders induced with plasma actuators. *Exp. Fluids* **2011**, *51*, 853–860. [CrossRef]

99. Artana, G.; Sosa, R.; Moreau, E.; Touchard, G. Control of the near-wake flow around a circular cylinder with electrohydrodynamic actuators. *Exp. Fluids* **2003**, *35*, 580–588. [CrossRef]

100. Hyun, K.T.; Chun, C.H. The wake flow control behind a circular cylinder using ion wind. *Exp. Fluids* **2003**, *35*, 541–552. [CrossRef]

101. Sung, Y.; Kim, W.; Mungal, M.G.; Cappelli, M.A. Aerodynamic modification of flow over bluff objects by plasma actuation. *Exp. Fluids* **2006**, *41*, 479–486. [CrossRef]

102. Kopiev, V.F.; Kazansky, P.N.; Kopiev, V.A.; Moralev, I.A.; Zaytsev, M.Y. HF DBD plasma actuators for reduction of cylinder noise in flow. *J. Phys. Appl. Phys.* **2017**, *50*, 475204. [CrossRef]

103. Sosa, R.; D'Adamo, J.; Artana, G. Circular cylinder drag reduction by three-electrode plasma actuators. *J. Phys. Conf. Ser.* **2009**, *166*, 012015. [CrossRef]

104. D'Adamo, J.; Leonardo, L.; Castro, F.; Sosa, R.; Duriez, T.; Artana, G. Circular Cylinder Drag Reduction By Three-Electrode Plasma Symmetric Forcing. *ASME J. Fluids Eng.* **2017**, *139*, 061202–061202-14. [CrossRef]

105. Zhang, X.; Choi, K.S.; Huang, Y.; Li, H. Flow control over a circular cylinder using virtual moving surface boundary layer control. *Exp. Fluids* **2019**, *60*, 104. [CrossRef]

106. Thomas, F.O.; Kozlov, A.; Corke, T.C. Plasma Actuators for Cylinder Flow Control and Noise Reduction. *AIAA* **2008**, *46*, 1921–1931. [CrossRef]

107. Konstantinidis, E.; Bouris, D. Vortex synchronization in the cylinder wake due to harmonic and nonharmonic perturbations. *J. Fluid Mech.* **2016**, *804*, 248–277. [CrossRef]

108. Feng, L.H.; Wang, J.J. Circular cylinder vortex-synchronization control with a synthetic jet positioned at the rear stagnation point. *J. Fluid Mech.* **2010**, *662*, 232–259. [CrossRef]

109. Feng, L.H.; Wang, J.J. Modification of a circular cylinder wake with synthetic jet: Vortex shedding modes and mechanism. *Eur. J. Mech. Fluids* **2014**, *43*, 14–32. [CrossRef]

110. Ma, L.Q.; Feng, L.H. Vortex formation and evolution for flow over a circular cylinder excited by symmetric synthetic jets. *Exp. Therm. Fluid Sci.* **2019**, *104*, 89–104. [CrossRef]

111. Jukes, T.N.; Choi, K.S. Control of unsteady flow separation over a circular cylinder using dielectric barrier discharge surface plasma. *Phys. Fluids* **2009**, *21*, 094106. [CrossRef]

112. Wang, C.; Tang, H.; Yu, S.C.M.; Duan, F. Lock-on of vortex shedding to a pair of synthetic jets with phase difference. *Phys. Rev. Fluids* **2017**, *2*, 104701. [CrossRef]

113. McLaughlin, T.; Munska, M.; Vaeth, J.; Dauwalter, T.; Goode, J.; Siegel, S. Plasma-Based Actuators for Cylinder Wake Vortex Control. In Proceedings of the 2nd AIAA Flow Control Conference, Portland, OR, USA, 28 June–1 July 2004. [CrossRef]

114. Konstantinidis, E.; Balabani, S. Flow structure in the locked-on wake of a circular cylinder in pulsating flow: Effect of forcing amplitude. *Int. J. Heat Fluid Flow* **2008**, *29*, 1567–1576. [CrossRef]

115. Perrin, R.; Braza, M.; Cid, E.; Cazin, S.; Chassaing, P.; Mockett, C.; Reimann, T.; Thiele, F. Coherent and turbulent process analysis in the flow past a circular cylinder at high Reynolds number. *J. Fluids Struct.* **2008**, *24*, 1313 – 1325. [CrossRef]

116. Kourentis, L.; Konstantinidis, E. Uncovering large-scale coherent structures in natural and forced turbulent wakes by combining PIV, POD, and FTLE. *Exp. Fluids* **2012**, *52*, 749–763. [CrossRef]

117. Jukes, T.N.; Choi, K.S. Long Lasting Modifications to Vortex Shedding Using a Short Plasma Excitation. *Phys. Rev. Lett.* **2009**, *102*, 254501. [CrossRef]

118. Xu, S.J.; Zhou, Y.; Wang, M.H. A symmetric binary-vortex street behind a longitudinally oscillating cylinder. *J. Fluid Mech.* **2006**, *556*, 27–43. [CrossRef]

119. Kim, K.H.; Choi, J.I. Lock-in regions of laminar flows over a streamwise oscillating circular cylinder. *J. Fluid Mech.* **2019**, *858*, 315–351. [CrossRef]

120. Feng, L.H.; Wang, J.J.; Pan, C. Proper orthogonal decomposition analysis of vortex dynamics of a circular cylinder under synthetic jet control. *Phys. Fluids* **2011**, *23*, 014106. [CrossRef]

121. Feng, L.H.; Wang, J.J. Synthetic jet control of separation in the flow over a circular cylinder. *Exp. Fluids* **2012**, *53*, 467–480. [CrossRef]

122. Ma, L.; Feng, L. Experimental investigation on control of vortex shedding mode of a circular cylinder using synthetic jets placed at stagnation points. *Sci. China Technol. Sci.* **2013**, *56*, 158–170. [CrossRef]

123. Liu, Y.G.; Feng, L.H. Suppression of lift fluctuations on a circular cylinder by inducing the symmetric vortex shedding mode. *J. Fluids Struct.* **2015**, *54*, 743 – 759. [CrossRef]